BMR RECORD 1987/49

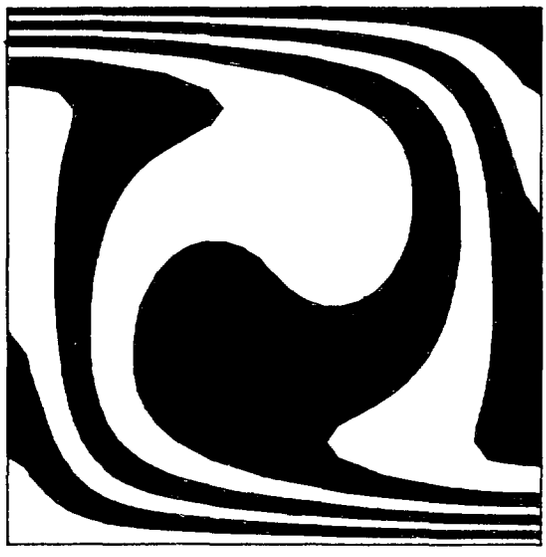

THE APPLICATION OF NUMERICAL TECHNIQUES IN EARTH SCIENCES

CONFERENCE ABSTRACTS, AUGUST 1987

COMPILED BY J. LEVEN, G. HOUSEMAN and C. COLLINS

RECORD 1987/49

The Application of Numerical Techniques in Earth Sciences

compiled by

J. Leven, G. Houseman, and C. Collins

Preface

This record is a compilation of the abstracts of papers presented at the "The Application of Numerical Techniques in Earth Sciences" conference held in Canberra on the 24-25 August, 1987.

The conference is sponsored by the Specialist Group on Solid-Earth Geophysics of the Geological Society of Australia, the Canberra Branch of the Australian Society of Exploration Geophysicists, the Research School of Earth Sciences, and the Bureau of Mineral Resources.

The conference aims to provide Earth scientists with a forum for the advancement of numerical modelling methods in geological and geophysical sciences. The application of these techniques to geological problems is rapidly developing, and knowledge obtained from modelling will prove important in our understanding of the fundamental processes in the Earth. We hope that by bringing together Earth scientists who are using numerical techniques in widely differing areas, they will benefit from the ideas and experience of others.

TABLE OF CONTENTS

NEW TWISTS IN THE EXTREMUM PRINCIPLES OF GEOMECHANICS

by Ian F. Collins

Department of Theoretical and Applied Mechanics

University of Auckland, New Zealand

Whilst the extremal principles of the mathematical theory of plasticity have been applied very successfully to analyse the deformation of metals, they have not met with the same success when applied to the deformation of soils and rocks. This is because the presence of internal friction in granular media leads to mathematical problems whose structure is not self-adjoint.

This paper will demonstrate that, when properly interpreted, these principles can be used to deduce much useful information in geomechanical engineering.

Three recent examples are discussed.

(a) The calculation of shakedown loads for bodies under cyclic loading. These loads serve as figures of merit for the design of pavements, roadways and airport runways. In the main the theory of shakedown has been developed and applied to frame structures. Such problems can be conveniently formulated as linear programming problems. However this procedure, at least in its primal form, is not nearly so attractive for continuum problems, because the number of constraints is now very large compared to the number of variables. In consequence in their analysis of the deformation of roadways under repeated loadings, Sharp and Booker (1984) developed an alternative procedure which they termed the "method of conics". Collins and Cliffe (1987) have recently reexamined the "method of conics" given it a kinematic interpretation and generalised the procedure to deal with much more realistic three-dimensional models. This parallels the corresponding investigations on the shakedown of metals by Ponter et. al. (1985). It is shown that this kinematic formulation is based on the dual extremal principle of shakedown theory. It has potential for generalisation to a wide range of problems involving cyclic loadings.

(b) There are very many studies of the stability of slopes in the soil mechanics literature. These are nearly all based on the Mohr-Coulomb failure criterion, which involves a linear relation between shear and normal stress. Whilst this criterion is appropriate for soils it does not model well the failure of closely jointed rock masses, which exhibit markedly nonlinear behaviour at failure. There is hence current interest in extending the classical soil stability analysis techniques to such non-linear materials - see for example Zhang and Chen (1987). The most widely used procedure is the "limit equilibrium" approach, which involves computing the overall equilibrium conditions for failing rock masses. This technique, though simple, is not based on any mechanical extremum principle, so that families of solutions cannot be systematically optimised. Techniques based on the classical extremum theorems of limit analysis are superior in this regard, though they are frequently critisised for the unrealistic normal flow rule assumption. However the significance of this assumption is not always fully appreciated, and, as shown by Collins et. al. (1987), these techniques can still be applied even though the real material behaviour deviates from that predicted by the normal flow rule.

(c) The upper bound techniques of limit analysis provide overestimates of failure loads - which are hence unsafe for design purposes. However when interpreted inversely they provide safe lower bound underestimates of material strength properties. Collins et. al. (1987) have recently systemised this procedure and shown that it is an example of the general "extremal stress field" concept introduced into stress analysis by Hill (1966).

I. F. Collins and P. F. Cliffe (1987) 'Shakedown in frictional materials under moving surface loads'. Int. J. Num, Anal. Methods in Geomechanics (in press).

I.F. Collins, C.I.M. Guun, M. J. Pender and Wang Yan (1987) 'Slope stability analyses for materials with a nonlinear failure envelope' (submitted for publication).

R. Hill (1966) 'The extremal stress-field concept' J. Mech. Phys. Solids 14, 239-243

A.R.S. Ponter, A.D. Hearle and K. L. Johnson (1985) 'Application of the kinematic shakedown theorem to rolling and sliding point contacts'. J. Mech. Phys. Solids, 33, 339-362.

R. W. Sharp and J. R. Booker (1984) 'Shakedown of pavements under moving surface loads'. J of Transportation Engineering, 110 - 1-14.

X. J. Zhang and W. F. Chen (1987) 'Stability analysis of slopes with general nonlinear failure criterion'. Int. J. Num. Anal. Methods in Geomechanics 11 33-50.

MECHANISMS AND ANISOTROPY IN ROCK MASS MODELLING

by B. CHAPPELL

Stress distribution and the flow of fluids are numerically modelled according to the differential equations and boundary conditions controlling deformation and fluid flow. These differentials are equations such as the elliptic and parabolic type equations. In addition to this, constitutive relations between stress and strain plus velocity and hydraulic head are required. The proportionality coefficients or parameters considered here are deformational moduli for stress and strain and permeability for velocity and hydraulic head. These parameters are a function of stress type (ie normal or shear stress) fluid condition (viscosity temperature) and the medium (namely rock mass) on and through which they act. In many instances the rock mass is foliated, with bedding and cross joints and faulted. These structural characteristics impose an anisotropy on the rock mass which controls both to stress distribution and fluid flow.

Besides controlling the stress distribution and fluid flow these anisotropies greatly effect the rock mass strength and fluid flow regime, laminar or turbulent flow.

For stress distribution the constitutive compliance parameter for a uniaxial load on an orthotropic rock mass is:

$$C_{my} = (C_u l^4 + C_L m^4) + l^2 m^2 [(Cg^u_{21} - Cg^L_{12}) - 2V_{12} C_L]$$

where l and m are sin 0 and cos 0 of the angle between the direction of the applied load and plane of anisotropy.
C_u and C_L composite compliance of the rock mass when the joint sets are perpendicular and parallel to the direction of the applied load,
Cg^u_{21} and Cg^L_{12} are the upper and lower bound shear moduli
V_{12} Poisson's ratio of rock mass.

For fluid flow the constitutive relation given by Darcy's equation is:

$$V_i = k_{ij} I_j S_{ij}.$$

when V_i is the velocity of fluid
I_j is the hydraulic head
k_{ij} is the coefficient of permeability
S_{ij} is kronecker delta.

In an orthotropic rock mass the format of parameters in the constitutive equations have similar characteristics except that in fluids shear dependency of the parameters does not exist. By examining the effect of shear on the anisotropic parameters some useful formulations for numerical modelling are obtained.

If shear modulus of the intact rock is neglected in the formulation of the rock mass modulus, the magnitude differences of the rock mass anisotropic moduli are markedly reduced. These anisotropic moduli differences are increased by the effects of shear stiffnesses or moduli.

In a fluid, shear stress is the internal force by which viscosity is defined, while pressure difference is the external force which drives the fluid. Depending on the geometrical configuration of the fluid flow direction to the layered material, the permeability magnitudes of the layered material are adjusted. Just as the anisotropic mass moduli in stress distribution are accentuated by the geometry of material and direction of imposed stresses so are the mass anisotropic permeabilities of the layered rock accentuated by the relative flow directions relative to the rock mass flow anisotropies.

In order to model these anisotropies the micro meso and macro aspects of the rock mass anisotropies need consideration. By lumping together these anisotropic characteristics using composite theory, it is possible to include many anisotropic features in the numerical characterisation of the rock mass. In addition, if other processes are caused by these anisotropies such as finite doformation or turbulent flow then additional modes of deformation or flow are readily superimposed and/or added to the original anisotropic processes. These additional mechanisms generally accentuate the original rock mass anisotropies.

COMPUTATIONAL STRESS ANALYSIS IN ROCK MECHANICS

M.A. Coulthard

CSIRO Division of Geomechanics, Mount Waverley, Vic. 3149

Introduction

Over the past 15-20 years computational stress analysis has become widely used in research in rock mechanics. Projects at the Division of Geomechanics have included, for example, studies of:

- deformation and stress changes associated with underground mine excavations in jointed rock;
- the mechanical behaviour of cemented mine fill;
- acoustic pulse transmission in rock; and
- surface subsidence induced by underground coal mining.

Because of the wide variation in rock types, structures and deformation mechanisms, no one numerical technique or computer program can accurately and efficiently model all the systems encountered in these areas of application. The rock mechanics research worker or design engineer therefore requires access to programs embodying a range of different techniques.

Some of the programs which have been developed, enhanced or used at the Division will be discussed in this paper, and the types of problem to which each is suited will be indicated.

Numerical techniques

Differential methods of stress analysis include finite element (FE), finite difference (FD) and distinct element (DE) methods. In these, the whole region being studied must be discretised into a mesh of elements and (somewhat arbitrary) displacement and/or stress boundary conditions must be applied to the periphery of the mesh to approximate the true boundary conditions at infinity. The FE and FD methods generally model rock as a pseudo-continuum, and are well suited to analysis of nonlinear behaviour such as rock mass yielding in shear or tension and large deformations. Highly jointed rock is modelled as a discontinuum in the DE method, which can handle gross relative displacements and rotations of rock blocks.

In contrast, integral or boundary element (BE) methods only require discretisation of boundaries - of excavations or of material zones - and automatically account for the exact boundary conditions at infinity. Such methods are very efficient in terms of data preparation and, particularly in 3-D, computer execution time, but are generally restricted to linearly elastic material behaviour and small deformations. The displacement discontinuity (DD) method is a special case of BE methods, and is designed for analysis of tabular excavations such as in underground coal mining.

Hybrid programs have been developed recently to capitalise on the relative advantages of these different methods. Usually, a differential method of analysis is used to model nonlinear behaviour in the near field, such as in the immediate vicinity of an excavation, with boundary elements being coupled to the periphery of the FE or DE region to represent the essentially elastic far-field rock behaviour and the boundary conditions at infinity. These can provide more efficient solution of many of the types of problem encountered in rock mechanics.

Two-dimensional stress analysis programs

Programs NTJTEP2 (Coulthard 1982) and BITEMJ (Crotty 1987) have been used extensively at the Division, mainly for analysis of excavations for underground metalliferous mining. NTJTEP2 is a plane strain FE code while BITEMJ is a BE program which can treat systems in plane strain or plane stress. Both have a simple Goodman joint element (Goodman et al., 1968) for modelling shearing or opening of major discontinuities in the rock mass. With BITEMJ, the rock mass may consist of several regions with different isotropic elastic properties, whereas NTJTEP2 can also model shear and tensile yield in bulk rock material. The application of these programs to the analysis of a faulted mine pillar was described by Coulthard et al. (1983); see Figure 1.

Several hybrid DE-BE computer programs have been enhanced at the Division recently. The most powerful, UDEC (Itasca, 1987b), can treat elastic and plastic deformations within each DE, fluid flow in the joints between them, rock support via grouted passive reinforcement, and structural elements for modelling tunnel linings. The capabilities of the others, HYDEBE and SDEBE, are given in their respective abstracts in Coulthard and Perkins (1987). Results from a UDEC demonstration calculation of ground caving and subsidence induced by underground coal mining are illustrated in Figure 2 (Dutton and Coulthard, unpublished).

The plane strain finite difference code FLAC (Itasca 1987a) was designed for analysis of systems exhibiting high degrees of material and/or geometric nonlinearity. Its capabilities will be described in another paper at this Conference (Price and Williams 1987).

A plane strain FE program, FESOFT, is being developed to model strain softening of geologic materials, such as yielding pillars in coal mines (Duncan Fama and Wardle, 1987).

Three-dimensional stress analysis programs

The general purpose FE program ADINA (Bathe 1978) has been used at the Division since 1979. It can treat static or dynamic loadings of 2-D or 3-D systems, includes a wide range of nonlinear material models and can model large displacements and strains. The latest version, ADINA84, has been released for royalty surcharge use on the Cyber 205 on CSIRONET. With vectorisation of the equation solution routines by CSIRONET, ADINA84 can be used to analyse very large systems relatively economically. ADINA studies have included the placement and exposure of cemented mine fill (Coulthard 1983) and elastic wave transmission through rock (Blair 1982, 1985). Some results from a dynamic verification analysis are shown in Figure 3.

Program MINLAY (Wardle 1984) is a DD code which can model the effects of complex 3-D excavation layouts in a single tabular orebody, in layered transversely isotropic elastic rock. The program includes a simple representation of yielding in pillars in the excavation plane, and will run satisfactorily on a personal computer. It has been used for back analysis of stress monitoring results from underground coal mines (Wardle and McNabb 1985 and Figure 4) and for studies of surface subsidence.

The hybrid BE-FE code BEFE (Beer 1986) is another program which has been vectorised and released for use on the Cyber 205. Nonlinear behaviour in rock near an excavation can be modelled using FEs, with BEs representing the far-field behaviour. Alternatively, complex multiple excavations in elastic rock can be modelled with BEs and slip on a fault plane analysed via coupled FEs, as in Figure 5.

Acknowledgements

The author appreciates the permission of several of his colleagues to include results from their work in this paper.

References

Bathe, K.-J. (1978) ADINA - A finite element program for automatic dynamic incremental nonlinear analysis. Report 82448-1, Department of Mechanical Engineering, Massachusetts Institute of Technology.

Beer, G. (1986) BEFE: Coupled boundary element - finite element program. In Structural Analysis Systems - 3 (ed. Niku-Lari), Pergamon Press, Oxford.

Blair, D.P. (1982) Dynamic modelling of in-hole mounts for seismic detectors. Geophys. J. R. astr. Soc., **69**, 803-18.

Blair, D.P. (1985) Acoustic pulse transmission in half-spaces and finite-length cylindrical rods. Geophys. **80**, 1676-83.

Coulthard, M.A. (1982) Plane strain nonlinear finite element program NTJTEP2 - Modifications and corrections for use in mining geomechanics. CSIRO Division of Applied Geomechanics, Technical Report No. 129.

Coulthard, M.A. (1983) Applications of ADINA in mining geomechanics. CSIRO Division of Applied Geomechanics, Geomechanics of Underground Metalliferous Mines Project Report No. 9 (unpublished).

Coulthard, M.A., Crotty, J.M. and Fabjanczyk, M.F. (1983) Comparison of field measurements and numerical analyses of a major fault in a mine pillar. Proc. 5th Int. Congress on Rock Mech., Melbourne, pp. D53-D60.

Coulthard, M.A. and Perkins, B.R. (compilers) (1987) Computer Program Abstracts - April 1987, 4th edition. CSIRO Division of Geomechanics, Technical Report No. 99.

Crotty, J.M. (1987) User's manual for program BITEMJ - two-dimensional stress analysis for piecewise homogeneous solids with structural discontinuities. CSIRO Division of Geomechanics, Geomechanics Computer Program No. 5, revision 3.

Duncan Fama, M.E. and Wardle, L.J. (1987) Numerical analysis of coal mine chain pillar stability. Proc. 6th Int. Congress on Rock Mech., Montreal.

Goodman, R.E., Taylor, R.L. and Brekke, T.L. (1968) model for the mechanics of jointed rock. Proc. A.S.C.E. Soil Mech. & Fndn. Engng. J. **93**, 637-660.

Itasca. (1987a) FLAC - Fast Lagrangian analysis of continua, version 2.00; User manual. Itasca Consulting Group, Inc., Minneapolis.

Itasca. (1987b) UDEC - Universal distinct element code, version ICG1.2; User manual. Itasca Consulting Group, Inc., Minneapolis.

Price, G.P. and Williams, P.F. (1987) Numerical modelling of simple shear deformation in an artificial salt-mica schist. Proc. Conf. on the Application of Numerical Techniques in Earth Sciences, Australian National University.

Wardle, L.J. (1984) Displacement discontinuity method for three-dimensional stress analysis of tabular excavations in non-homogeneous rock. Proceedings 25th U.S. Rock Mechanics Symp., Evanston, pp. 702-709.

Wardle, L.J. and McNabb, K.E. (1985) Comparison between predicted and measured stresses in an underground coal mine. Proceedings 26th U.S. Rock Mechanics Symp., Rapid City, pp. 531-538.

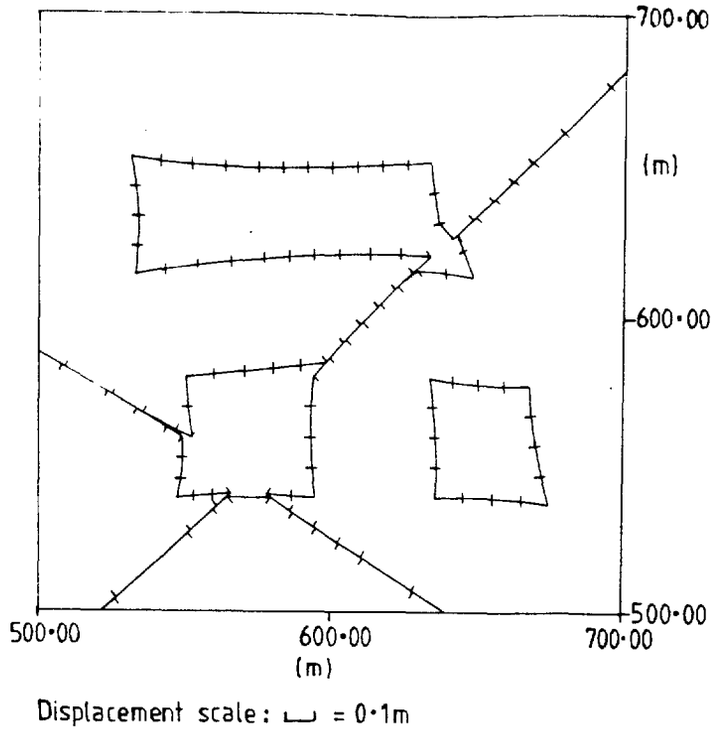

Figure 1. Rock movements induced by multiple excavations in jointed rock, as calculated with program BITEMJ.

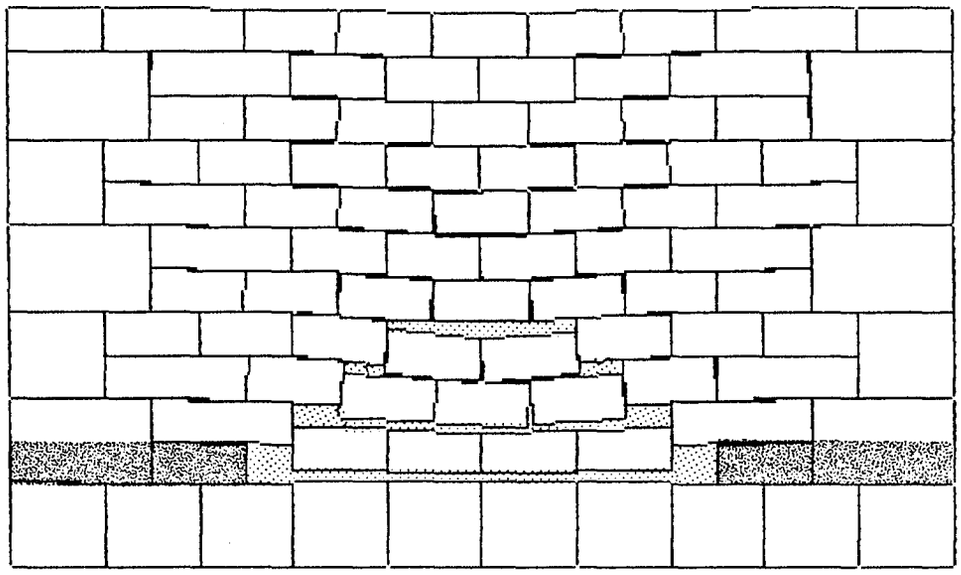

Figure 2. Results from UDEC modelling of roof caving and ground subsidence.

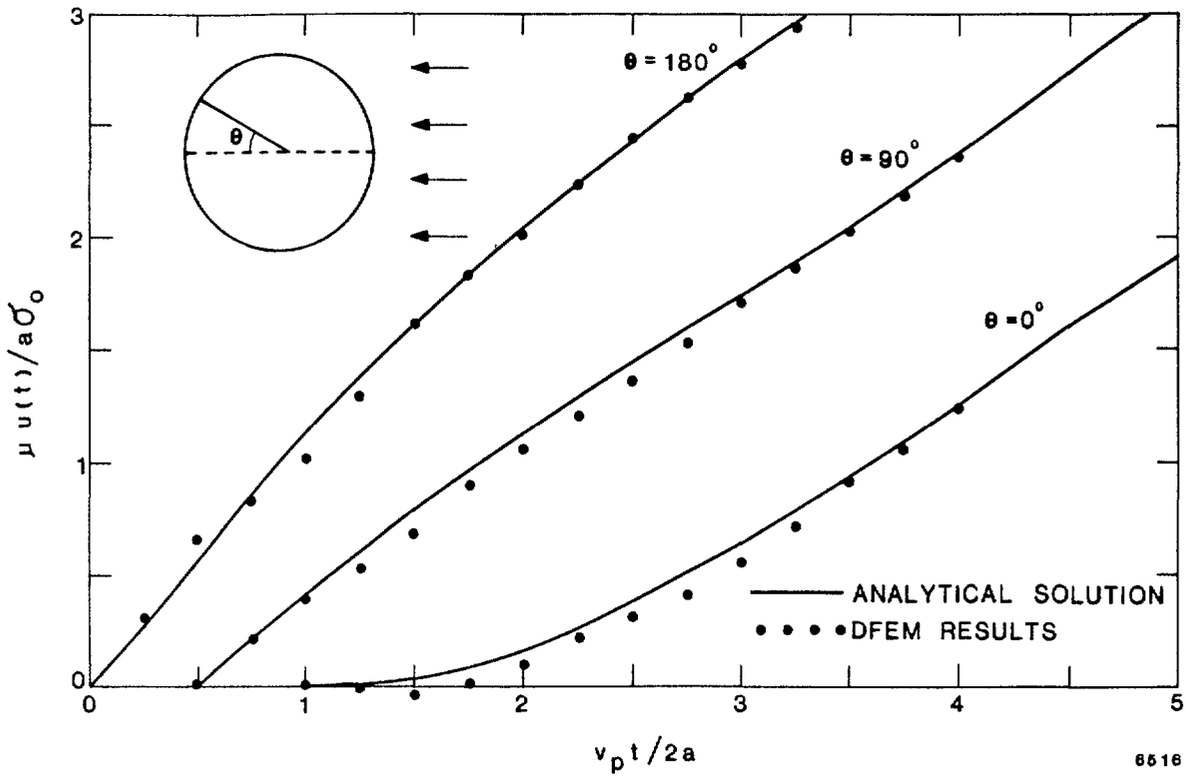

Figure 3. Displacement response of a cylindrical cavity to an incident 'shock' wave.

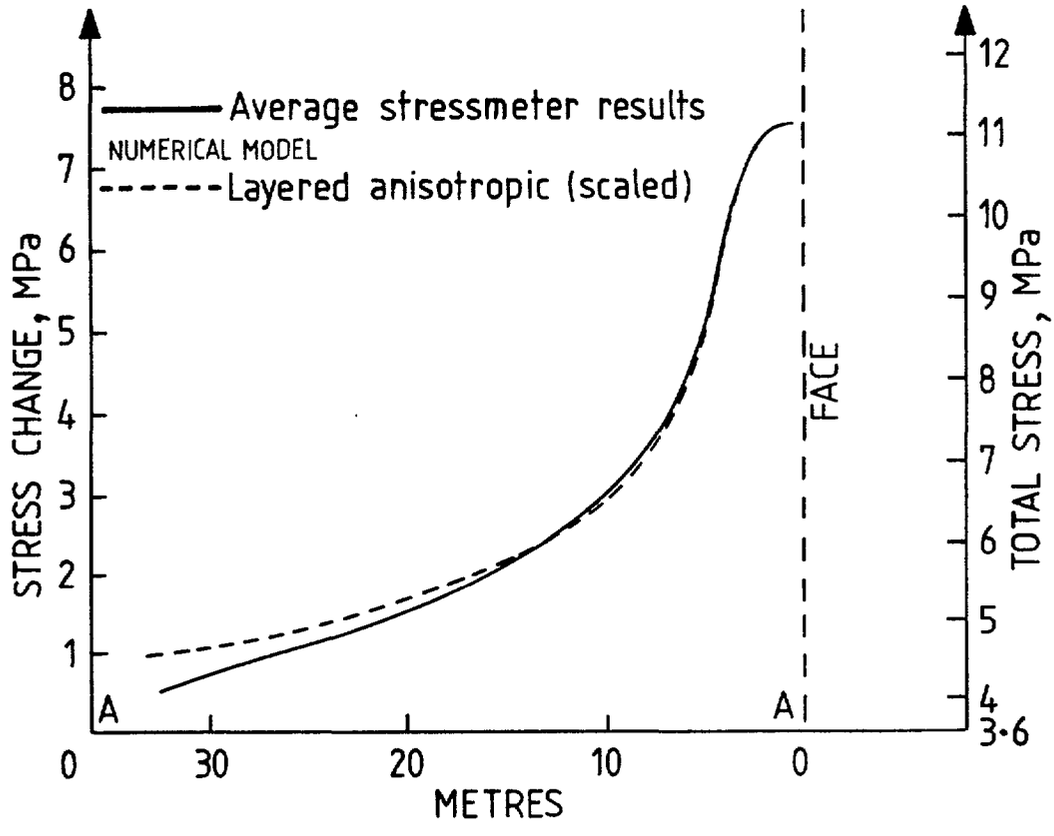

Figure 4. Measured stresses ahead of a longwall mining face compared with those calculated with program MINLAY.

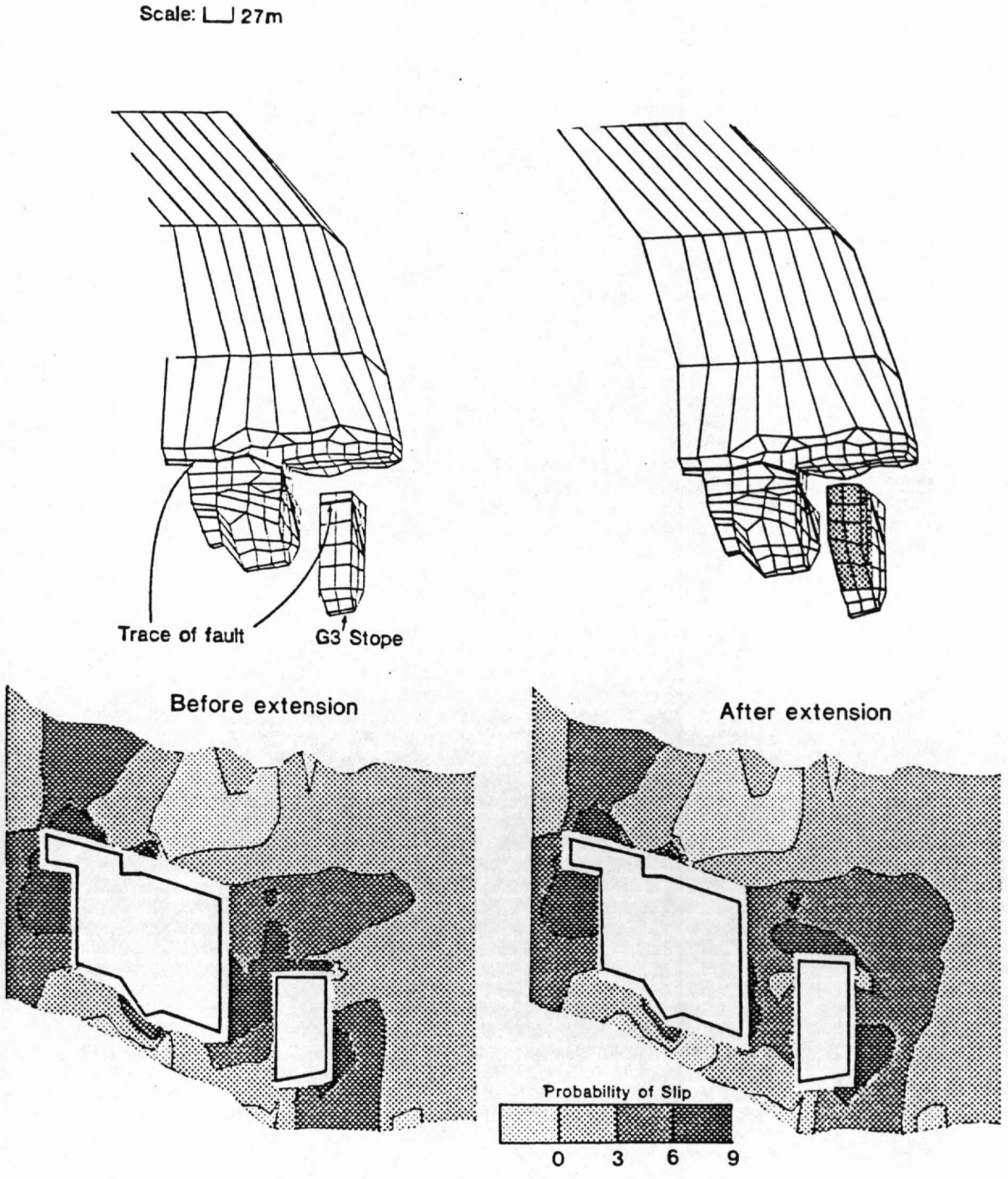

Figure 5. Mining excavation in faulted rock and probability of slip on fault plane, as calculated with program BEFE.

REACTIVATION OF BASEMENT FAULTS: 2-D PLANE-STRAIN MODELLING USING ADINA

Jim Leven

Bureau of Mineral Resources, Geology and Geophysics

Several recent and important oil discoveries in the Eromanga Basin have been made within structural traps created by tectonic reactivation of pre-existing Palaeozoic basement faults. Two styles of basement fault reactivation are observed. The first involves virtually no deformation within the basement hanging wall block, and consequently no structuring on the overlying sedimentary sequence except directly over the fault. This style of structuring is unlikely to produce any significant petroleum traps. The second style involves deformation within the hanging wall block and consequent structuring of the overlying sedimentary sequence. Figure 1 shows compressive reactivation of a basement fault forming a ramp anticline in the overlying sedimentary sequence.

Such ramping of the overlying sedimentary sequence can both create and destroy anticlinal traps. If the stress produced in the overlying strata during deformation exceeds the strength of the rock, then crestal faulting will result, thereby breaching the structural trap. Any oil accumulated in the trap may then leak from the trap.

The relatively uniform stratigraphy of the Eromanga Basin sequence allows the tectonic reactivation of this second style to be modelled by numerical techniques. The ADINA finite element program installed on the CSIRONET Cyber 205 computer (ADINA Users Manuals, 1984) can be used for this modelling. Although specifically designed for non-linear analysis, ADINA can cope with static linear problems of the style mentioned above. For this two dimensional plane-strain problem, the stress-strain equations reduce to (Turcotte and Schubert, 1982):

$$\sigma_1 = (\lambda + 2\mu)\varepsilon = \lambda\ \varepsilon_2$$
$$\sigma_2 = \lambda\ \varepsilon_1 + (\lambda + 2\mu)\varepsilon_2$$

where σ and ε are the stress and strains respectively for the principal directions, λ and μ are the Lame parameters. Calculations of the stresses that result in a linear isotropic homogeneous elastic model of the Mesozoic sequence with prescribed base displacements equal to those observed in the ramp anticline structures have been made. The ADINA program calculates displacements and principle stresses σ_1 and σ_3 at each node.

For this analysis, it was assumed that the sedimentary sequence behaves in a linear elastic manner. The results are particularly dependent on the rheology and material properties used. Measurements of the density are available, and the Poisson's ratio can be constrained to within a reasonable range from measurements of other sandstones and shales. Although Young's modulus is not constrained directly, measurements of the P and S wave velocities of samples from the Tintaburra well (D. King, pers. comm.) have been used to obtain an estimate of Young's modulus. The variation of this modulus with pressure has not been incorporated into the modelling due to lack of data.

The Mohr failure criterion (Jaegar, 1969) predicts failure to occur when the Mohr stress circle intersects the failure envelope. Data from triaxial failure experiments on the various rock types from the Eromanga Basin are not available. Published values of rock strength (Handin, 1966; Blanic and others, 1981) have therefore been used to estimate a failure envelope for typical sandstones and shales. An empirical quadratic curve was used to characterize this envelope (Figure 2):

$$\sigma_n = \frac{\sigma_s^2}{69} - 5 \qquad \text{where stresses are in MPa.}$$

Using this failure criterion, the principal stresses calculated by the ADINA program were used to calculate the percentage of the ultimate strength that the maximum shear stress reaches during elastic deformation for each element in the model.

Better determination of the material properties of sedimentary rocks will enable this modelling technique to evaluate whether a structural trap is likely to have been breached by the development of crestal faulting prior to drilling.

References.

ADINA Users Manual and ADINA Theory and Modelling Guides. Reports AE84-1 & AE84-4, ADINA Engineering.

Blanic, J.D., Halleck, P.H., D'Onfro, P., & Riecker, R.E., 1981. Thermomechanical Properties of the Galesville Sandstone. In: Mechanical Properties of Crustal Rocks (Handin Volume) Geophysical Monograph 24, Am. Geophys. Union, pp 153-159.

Handin, J., 1969. Strength and Ductility. in: Handbook of Physical Constants. Ed: S.P. Clark, Memoir Geol. Soc. Am., 97, pp 223-289

Jaeger, J.C., 1969. Elasicity, Fracture and Flow. Methuen.

Turcotte, D.L., & Schubert, G., 1982. Geodynamics - Applications of Continuum Physics to Geological Problems. John Wiley and Sons.

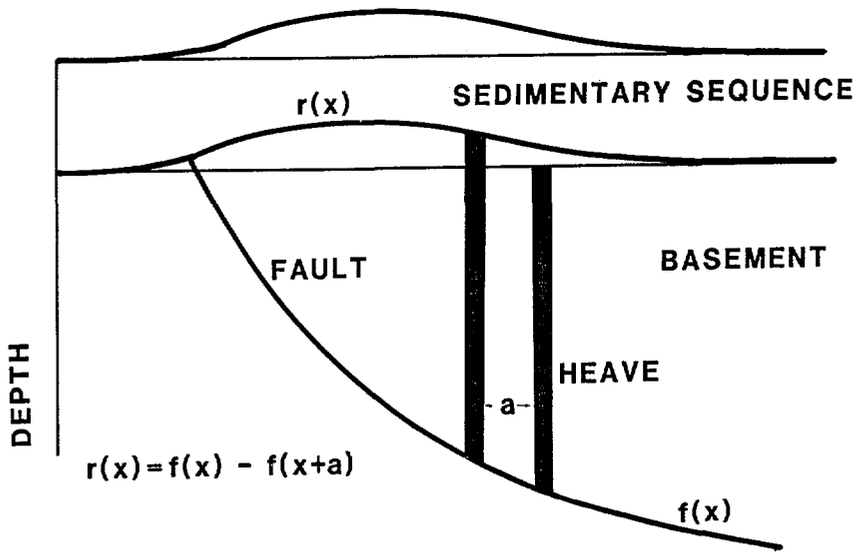

Figure 1. Model of compressive reactivation of a basement fault with simple shear deformation in the hanging-wall block and no deformation in the footwall. A ramp anticline structure is formed in the over-lying sedimentary section by this reactivation.

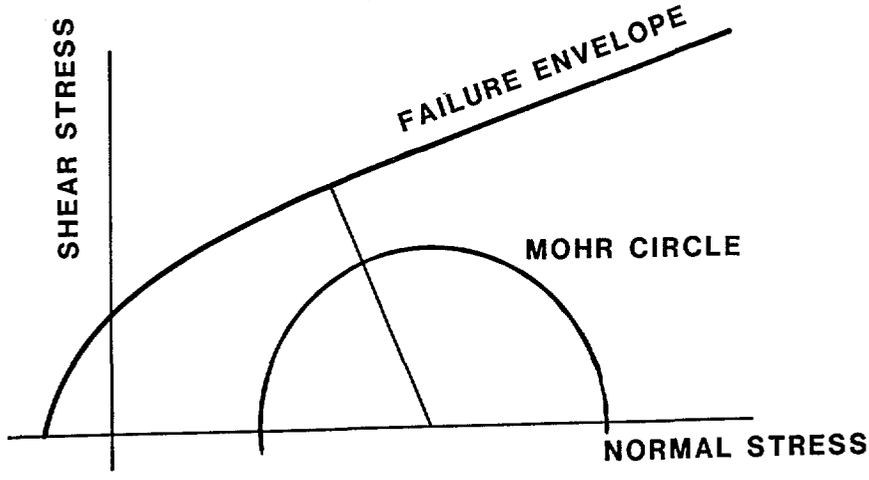

Figure 2. The Mohr circle for given values of the maximum and minimum stress, and the failure enevelope which determines the maximum shear stress for a particular maximum normal stress.

NUMERICAL MODELLING OF SIMPLE SHEAR EXPERIMENTS IN AN ARTIFICIAL SALT-MICA SCHIST

Graham P. Price[1] and Paul F. Williams[2]

[1] CSIRO Division of Geomechanics, Mt Waverley, 3149 Australia
[2] Dept. of Geology, University of New Brunswick, Fredericton, New Brunswick, Canada

An experimental programme was conducted, involving simple shear deformation of artificial salt-mica schists using a new plane strain simple shear apparatus developed at the Division of Geomechanics in Melbourne. The objective of this study was to investigate the effect of changes in fabric orientation on the deformation mechanisms and the microstructures produced in a strongly anisotropic material.

The specimens for this study were rectangular blocks (60mm x 50mm x 48mm) of artificial salt-mica schist composed of a mixture of 70% by weight salt (NaCl or KCl) and 30% by weight muscovite mica. The blocks were cut such that a strong foliation, defined by parallel alignment of mica flakes, was inclined at various angles to the intended horizontal shear plane and intersected the shear plane normal to the shear direction. Each of the specimens was decorated with strain markers on the vertical faces normal to the shear plane and parallel to the shear direction. Experiments were carried out with the mica foliation varying in 10^{o} steps from parallel to the shear plane, through the normal to the shear plane and back to parallel. Additional experiments were conducted to investigate the effects of different strain rates, different stresses normal to the shear plane and different grainsizes of the salt and mica.

Thin-sections were prepared from each specimen after deformation and the fabrics examined with an optical microscope. Specimens in which the foliation lay in, or on the margins of, the shortening field relative to the principal stress ellipsoid for this shear deformation (foliation angles 0^{o} to 90^{o}, see figure), developed either one set of kink bands or a conjugate pair of kink bands. One of the kink bands is in a steep orientation close to the normal to the shear plane and the other in a shallow orientation close to the shear plane. The changes, from one set of steep kink-bands to a conjugate pair and back to one set of shallow kinks, occur systematically as the initial foliation orientation changes from 0^{o} to 90^{o}. Specimens in which the foliation lay in the extension field (foliation angles 100^{o} to 170^{o}) developed either one set of shear-band cleavages or a conjugate pair of shear-band cleavages. As with the kink-bands one set of shear-band cleavages is steep close to the shear plane normal and the other set is shallow close to the shear plane. The change, from one cleavage to the conjugate pair and then to the other cleavage, is systematic and correlates with changes in the foliation orientation from 100^{o} to 170^{o}.

To support this experimental work the simple shear experiments were modelled numerically with the objective of assessing the suitability of the modelling codes for this type of anisotropic material and of exploring the effects of experimental conditions which were not used in the laboratory experiments. A general purpose, geomechanical, finite difference code called FLAC (Fast Lagrangian Analysis of Continua), produced and marketed by Itasca Consulting Group Inc, Minneapolis, USA, was selected. This code allows the use of a homogeneous Mohr-Coulomb plasticity material model for the salt combined with an embedded set of ubiquitous joints (in geological term penetrative joints) to represent the mica foliation. Only the salt-mica specimens were modelled and not the apparatus. Progressive simple shear deformation was achieved by applying boundary displacement conditions equivalent to a constant shear strain rate with no dilation. Since the real material properties of the

salt-mica specimens were not initially known a reasonable set of material properties was chosen in which the yield stresses of the salt and the mica foliation were about equal.

The numerical models produced strain patterns with strong similarities to those in the salt-mica specimens for those experiments where the foliation lay in, or on the margins of, the shortening field. Kink bands were the dominant deformation mechanism with a set of steep kinks when the initial foliation was low, a set of inclined kinks approximately normal to the foliation when it is at intermediate angles and a set of shallow kinks when the foliation is high. The models for specimens with the foliation in the extension field did not produce any localised structures and certainly not the shear band cleavage type structures as occurred in the experimental specimens. For these experiments with the foliation in the extension field the material model used seems to be inappropriate. A later version of FLAC does have a strain softening material model and it is anticipated that this will lead to a better simulation of the experimental structures.

Although the kinks in the numerical model do not exactly replicate the conjugate kink pair produced in the experimental specimens the fact that kinks formed at all was a surprising result. Kink bands are a form of strain localisation or bifurcation phenomena and this type of behaviour has not been readily reproduced with numerical models before. It appears that this type of behaviour arises because of a delicate balance which is established within the model during shear deformation. This balance is between the capacity of an individual cell to achieve the imposed shape change by plastic deformation of the continuum or to achieve it by sliding on the ubiquitous joints.

The Mohr-Coulomb plastic rheology requires that a critical value of shear stress be developed before plastic deformation can initiate. The orientation of that shear stress, determined by the orientation of the principal stresses, is not important nor is the mean stress. If the shear stress is not sufficient then the cell will only deform elastically even if the mean stress is high, but if the shear stress is sufficient then the cell will deform plastically and any arbitrary shape change can be achieved. Plastic deformation also passively rotates an embedded ubiquitous joint set as it would for any line of material points in a shear deformation. In contrast slip on an ubiquitous joint set will be activated only if sufficient shear stress is resolved onto the particular joint orientation. Hence the orientation of the principal stresses is important. Slip on a ubiquitous joint set can achieve only a specific change in shape and this may not satisfy the imposed displacement conditions. Also deformation by slip on a ubiquitous joint set does not rotate the joint set.

A material model, such as this Mohr-Coulomb continuum plasticity plus the ubiquitous joint set, therefore has two possible deformation mechanisms and the balance between the activity of these two mechanisms is postulated as the cause of the observed localised deformation heterogeneity. Numerical codes do exist which allow more than two deformation mechanisms however the behaviour of these have not been explored. It appears that the potential now exists for a wide range of material behaviour to be modelled numerically and increased interest is anticipated in this field

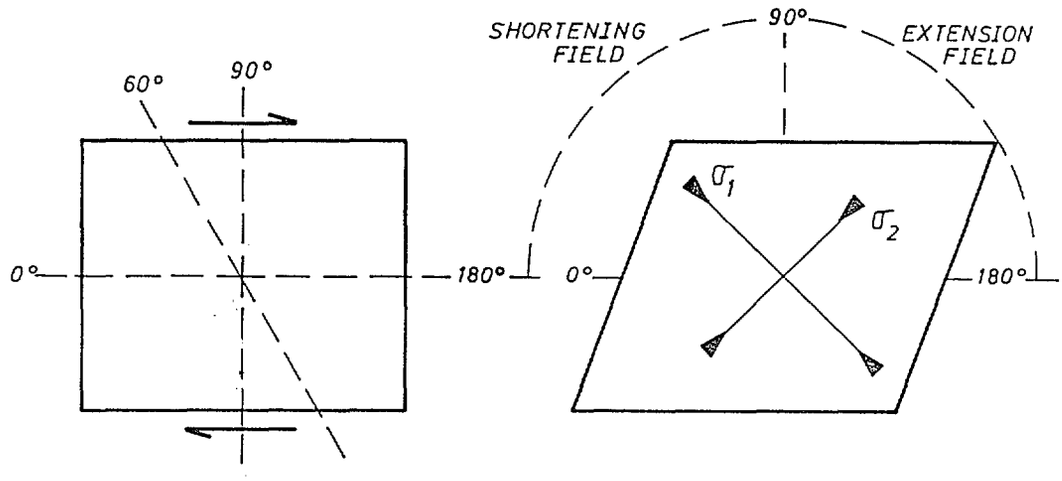

CREEPING MANTLE FLOW WITH LARGE VISCOSITY VARIATIONS: FINITE DIFFERENCE METHODS AND ITERATIVE SOLUTIONS

Geoffrey F. Davies

Research School of Earth Sciences, Australian National University
Canberra

Large viscosity gradients are a fundamental feature of flow in the earth's mantle. They arise because of the strong temperature-dependence of silicate rheology: at mantle temperatures of about 1400°C, a change of temperature by 100°C induces a change in viscosity by nearly a factor of 10. With thermal boundary layers about 100 km thick, we get viscosity gradients of the order of a factor of 10 per 10 km, compared with length scales of the flow of the order of 1000 km. Such gradients pose a considerable numerical challenge.

In fact, we do not have to allow for 14 or more orders of magnitude of viscosity variation. Viscosities that differ by more than 3 or 4 orders of magnitude from viscosities away from the boundary layers will induce effectively rigid or inviscid behaviour, and larger excursions can be clipped at these values. Nevertheless, the transitions to high or low viscosity will still involve large gradients.

These problems are encountered during numerical modelling of thermal convection in the mantle. The most significant other parameters are the high viscosity (about 10^{21} Ns/m or 10^{22} poise) and the moderately high Rayleigh number (about 10^7). The heat equation is not affected by variable viscosity, and standard methods are used. Discussion here will focus on the flow equation, which can be written in terms of a stream function, ψ, as follows:

$$[\eta(\psi_{xx} - \psi_{yy})]_{xx} - [\eta(\psi_{xx} - \psi_{yy})]_{yy} + 4[\eta\psi_{xy}]_{xy} = T_x \qquad (1)$$

where η is the viscosity, T is the temperature and subscripts x and y denote partial derivatives. Two alternative forms are possible. One has a pure biharmonic operator on the left side:

$$\eta\Delta^4\psi = T_x + (\eta_{xx} - \eta_{yy})(\psi_{yy} - \psi_{xx}) - 4\eta_{xy}\psi_{xy} - 2\eta_x(\psi_{xxx} + \psi_{xyy}) - 2\eta_y(\psi_{xxy} + \psi_{yyy}) \qquad (2)$$

The other form splits the equation into two Poisson equations, but this form will not be considered here (it is useful if only stress boundary conditions are used, but requires extra iteration if velocity boundary conditions are required).

Two methods of solving the flow equation will be illustrated here. The first is a simple iteration based on equation (2). The second is an alternating-direction implicit (ADI) method applied to equation (1), augmented by a conjugate gradient iterative acceleration. Some possible variations on the latter will be mentioned.

For moderate viscosity contrasts (up to about 100 in the examples considered here), equation (2) enables a reasonably efficient solution,

because the biharmonic equation can be solved very efficiently. Since the stream function gradients are not known a priori, iteration on the right side of (2) is necessary. One of the more efficient ways to solve a biharmonic equation is to use fast Fourier transforms. The method is a direct extension of transform methods used for the Poisson equation (Buzbee and Dorr, 1974; Swarztrauber, 1977). Transforming each row of the grid yields a set of pentadiagonal matrices which can be solved efficiently using specialised Gaussian elimination. Any combination of stress and velocity boundary conditions is readily accomodated. For constant viscosity viscous flow problems, where the right-hand stream function terms in (2) vanish, this method allows an efficient direct solution.

The iteration of (2) can begin with the right-hand stream function terms set to zero. Succeeding iterations need to be damped to preserve convergence for grids larger than about 32x32 and viscosity contrasts greater than about 5. Damping consists of adding only part of the change from one iteration to the next. If n is an iteration index, then

$$\psi^{n+1} = (1-a)\psi^{n} + a\psi^{*n+1} \qquad (3)$$

where a is a damping factor ($0 \leq a \leq 1$) and ψ^{*n+1} is the undamped solution. Greater damping (smaller a) is needed for larger grids and larger viscosity contrasts. This method has been used on grids up to 64x256 with viscosity contrasts up to 100, but by then $a \leq 0.2$ is needed and over 100 iterations can be required. Worse, the iterations do a slow oscillation. Establishing convergence becomes a serious problem. Typically, the criterion used was a relative change of less than 10^{-3} or 10^{-4} between iterations, but of course this depends on the application.

For reasons not understood, the method performed much worse with a zero stress top boundary (the above description applies to a prescribed velocity top boundary with zero stress on the other boundaries). Convergence failed for viscosity contrasts greater than about 5.

Alternating direction methods are a general class of methods in which a partial differential equation is split into a set of ordinary differential equations, one per dimension. These are then cycled through iteratively. The method can be applied to almost any equation, and has the additional advantages of moderate efficiency and modest storage requirements. There are many possible variations, even for a given equation (Lapidus and Pinder, 1982).

An alternating-direction implicit (ADI) method for equation (1) was proposed by Houston and De Bremaecker (1974) based on an ADI splitting for the biharmonic equation proposed by Conte and Dames (1958). This splitting is

$$\psi^{n+1} = \psi^{n} + r[T_x - (\eta\psi^{n+1}|_{yy})_{yy} + (\eta\psi^{n}|_{xx})_{yy} + (\eta\psi^{n}|_{yy})_{xx} - (\eta\psi^{n}|_{xx})_{xx} - 4(\eta\psi^{n}|_{xy})_{xy}] \qquad (3a)$$

$$\psi^{n+2} = \psi^{n+1} - r[(\eta\psi^{n+2}|_{xx})_{xx} - (\eta\psi^{n}|_{xx})_{xx}] \qquad (3b)$$

where the derivative notation denotes finite difference approximations. Equation (3a) is implicit in y and equation (3b) is implicit in x. This is not an obvious way to split equation (1), and Conte and Dames did not reveal their rationale, but trials have revealed that it gives more rapid convergence than more obvious splittings. However, errors accumulate more rapidly, so double precision is necessary for all but the smallest grids.

The factor r is analogous to a time step, and its value may be varied with both iteration number and position. In fact, it was written as $r = \omega/c_{ij}$, where c_{ij} is the coefficient of ψ^{n+1}_{ij} in the right-hand side, and ω is independent of position. The value of ω is important, and the value which optimises convergence is best found empirically. Different values of ω cause different wavelengths of the solution to converge fastest, so a better procedure is to cycle through a range of values of ω in successive iterations.

Even so, the ADI method is still unsatisfactory with large grids (64x256). It was found that the conjugate gradient method can be used as an accelerator to speed convergence by a factor of about 6. The difference form of equation (1) can be written as a matrix equation

$$\underline{A}\underline{x} = \underline{b} \qquad (4)$$

where $\underline{x}$ is a vector of all the unknown values on the grid. The conjugate gradient method (Reid, 1971) is based on minimising the associated quatratic form

$$f(\underline{x}) = \underline{x}^T\underline{A}\underline{x}/2 - \underline{b}^T\underline{x} \qquad (5)$$

which also minimises the residue

$$\underline{r}^n = \underline{b} - \underline{A}\underline{x}^n \qquad (6)$$

where $\underline{x}^n$ is the n^{th} approximation to $\underline{x}$. The vector which minimises (5) can be written as the sum of a series of orthogonal vectors which can be defined by a Gram-Schmidt procedure. The simplest conjugate gradient method simply uses the first vector in this series, defined as orthogonal to $\underline{r}^n$, at each iteration. The conjugate gradient method so defined could itself be used as an iterative solution method, but it also tends to be slow to converge for large problems.

It has been found that the conjugate gradient method can be combined with other iterative methods with results superior to either used separately (Kershaw, 1978; Khosla and Rubin, 1981). Suppose M is a matrix which approximates A and is "easy" to solve. An example is the matrix expression of equations (3). Then M^{-1} can be used to "precondition" A, in effect minimising the residue

$$\underline{e}^{n+1} = \underline{x}^{n+1} - \underline{x}^n = M^{-1}\underline{b} - M^{-1}\underline{A}\underline{x}^n \qquad (7)$$

This is accomplished by solving

$$\underline{M}\underline{e}^{n+1} = -\underline{r}^{n} \qquad (8)$$

Since (8) is equivalent to solving equations of the form (3), the ADI method is integrated into the conjugate method.

Comparisons of convergence behaviour will be given. More important, in the light of experience with the first iterative method described above, this method seems to be very robust. Solutions have been obtained with a zero-stress top boundary and viscosity variations of a factor of 100. With a velocity boundary condition, viscosity variations of at least 1000 are possible, but the limits have not yet been explored. Furthermore, convergence seems to be monotonic, although about 100 iterations may be necessary.

The matrix M can represent any approximation to A, and in fact other examples were used in the references cited above. Khosla and Rubin used the "strongly implicit" (SI) method (Stone, 1968; Jacobs, 1973), which is a special case of the "incomplete Cholesky" (IC) method used by Kershaw. Combined with conjugate gradients, the latter methods have impressive speed and robustness properties. The basis of these methods is an approximate LU decomposition of M (where L and U have lower- and upper-triangular form, respectively) such that L and U between them have elements in the same positions as in M. In general, the product LU then has more elements, but they can be chosen such that the extra elements are small. Thus, LU approximates M and is, of course, readily soluble. The SI method is the specialisation of IC to band matrices.

References

Buzbee, B.L. and F.W. Dorr, SIAM J. Numer. Anal., 11, 753-763 (1974).

Conte, S.D. and R.T. Dames, Math. Tables Aids Computation, 12, 198-205 (1958).

Houston, M.H. and J.C. DeBremaecker, J. Comput. Phys., 16, 221-239 (1974).

Jacobs, D.A.H., J. Comput. Phys., 13, 303-315 (1973).

Kershaw, D.S., J. Comput. Phys., 26, 43-65 (1978).

Khosla, P.K. and S.G. Rubin, Computers and Fluids, 9, 109-121 (1981).

Lapidus, L. and G.F. Pinder, Numerical Solution of Partial Differential Equations in Science and Engineering, Wiley, 677pp. (1982).

Reid, J.K., in Large Sparse Systems of Linear Equations, edited by J.K. Reid, Academic Press, London, p. 231-253 (1971).

Stone, H.L., SIAM J. Numer. Anal., 5, 530-558 (1968).

Swarztrauber, P.N., SIAM Review, 19, 490-501 (1977).

Long wavelength gravity and topography with variable viscosity: A finite element approach

Mark A Richards
University of Oregon, Eugene, Oregon

The Earth's gravity anomalies are dominated by the very longest wavelength components, namely harmonic degrees 2 and 3. Recently, I have developed models for these components based upon low-degree density contrasts in the mantle inferred from seismic tomography. These spherical Earth models include the gravitational effects of deformation of the surface and core-mantle boundary due to buoyancy driven flow in the mantle, and also include the effects of radial viscosity variations in the mantle. In order to understand the effects of lateral viscosity variations (expected to accompany lateral temperature and density variations), I have used 2-D finite element models of flow due to specified buoyancy distributions and due to thermal convection.

The results of these numerical experiments are remarkably straightforward: For the very longest-wavelength mantle density contrasts (wavelength >> mantle depth), the topography and gravity signatures are almost insensitive to lateral viscosity contrasts. Shorter-wavelength (harmonic degrees $\geq$ 4) may be seriously contaminated by the effects of temperature and/or stress dependent viscosity. This effect may be observable at degree 4. and it may explain why the shorter-wavelength gravity anomalies cannot be modeled very successfully.

THREE-DIMENSIONAL SOLUTIONS OF THE CONVECTION EQUATIONS: APPLICATION TO THE EARTH'S MANTLE.

Gregory A. Houseman

Research School of Earth Sciences, Australian National University, G.P.O. Box 4, Canberra, A.C.T., 2601.

Using a vector potential formulation for the velocity field,

$$\underset{\sim}{V} = \underset{\sim}{\nabla} \times \underset{\sim}{A}$$

($\underset{\sim}{V}$ is velocity, $\underset{\sim}{A}$ is the stream function), the momentum equation for a constant viscosity, infinite Prandtl number, fluid can be written as a biharmonic equation, in which the source terms are proportional to the horizontal gradients of temperature:

$$\nabla^4 \underset{\sim}{A} = R \left[\frac{\partial T}{\partial y} \underset{\sim}{\hat{x}} - \frac{\partial T}{\partial x} \underset{\sim}{\hat{y}} \right]$$

(R is the Rayleigh number, T is temperature, $\underset{\sim}{\hat{x}}$ and $\underset{\sim}{\hat{y}}$ are the unit horizontal vectors). The evolution of the temperature field is determined by the conservation of energy equation:

$$\frac{\partial T}{\partial t} + \underset{\sim}{V} \cdot \nabla T = \nabla^2 T + \mu$$

(t is time and μ is a dimensionless internal heating rate). These equations can be solved for the temperature and velocity fields by timestepping from time level n to time level n+1, from an initial temperature field (n=0), onwards.

Because the biharmonic equation must be inverted at least twice every timestep, the key to an effective three-dimensional convection program is a fast routine for inversion of the biharmonic operator. The technique is relatively straightforward: Fourier transforms in the horizontal directions, followed by cyclic reduction of the resulting ordinary differential equations in z (for each horizontal wavenumber), followed by inverse Fourier transforms. It is now feasible to accelerate this process to solve large problems in short times (e.g. 129 × 129 × 33 = 549,153 mesh points in $\frac{1}{2}$ second) by using the vector processor capacity of modern supercomputers. To make best use of the vector pipeline, the 3-dimensional array must be stored so that the longest possible vectors can be used in each operation. E.g., for the x-direction Fourier transform, these vectors consist of y-z planes, requiring that the mesh points be indexed in the order (y, z, x). Similarly for the y-direction transform and the z-direction cyclic reduction the vectors for the operation consist of the planes orthogonal to the direction of the operation. This choice of mesh point indexing is called orthogonal vectorisation. It requires that the entire 3-dimensional work matrix be transposed 4 times during the solution of the biharmonic equation.

An explicit finite difference approximation may be used for the energy equation. In advancing the temperature at each mesh point, the temperatures at the six nearest neighbour points (separation h) at two time levels are required, as are streamfunction values from 8 of the next-nearest neighbour mesh points (separation $\sqrt{2}$ h). The expression is unwieldy but straightforward. The size of the timesteps must be $^1/_3$ less than in an equivalent two-dimensional calculation.

High Rayleigh number convection experiments run in 4 × 4 × 1 boxes show several different types of convection planform, with both axial and elongate sheet structures present. The type of planform is dependent on heating mode (among other things). For an internally heated fluid the planform is dominated by cold axial sinkers that form by instability of the upper thermal boundary layer. When half of the heat is from below and half is generated internally the preferred planform consists of hot rising axial plumes and cold elongated sinking sheets. Both solutions are strongly time-dependent.

NUMERICAL TECHNIQUES IN ELECTROMAGNETIC INDUCTION AND MODELLING THE GEOMAGNETIC COAST EFFECT IN 2-D.

Richard Kellett

Research School of Earth Sciences, Australian National Univ., Canberra

In natural-source electromagnetic induction studies, fluctuations of the earth's magnetic and electric fields are measured using an array of stationary instruments. The fields result from the flow of electric currents both internal and external to the earth. At periods between one minute and one day, the external field is assumed to have a wavelength much greater than the length scale of the region of the earth being investigated. This assumption, combined with techniques which can separate the internal and external fields, allows the distribution of internal electric current to be determined. The electric conductivity structure is directly related to the current distribution and is interpreted in terms of geology.

The analysis of magnetic field fluctuations often indicates that there is a large anomalous part in the vertical component, especially near coastlines. This phenomenon is known as the Geomagnetic Coast Effect. The presence of anomalous vertical field is an indication that the underlying earth is not one-dimensional. In many cases two-dimensional models have been used to describe the electric conductivity very successfully.

Electromagnetic induction at these periods is a diffusion phenomenon so the equations which describe the distribution of electric and magnetic fields in both time and space are similar to the heat equation. These equations divide into two groups for the two-dimensional case. One group applies when the source magnetic field is polarised parallel to the strike of the model. This case is known as the "H-polarisation", and involves only components H_x, E_y and E_z (where x is the axis parallel to the strike of the model). The second group is known as "E-polarisation", and involves only the components E_x, H_y and H_z. The two modes can be treated separately. The behaviour of the components of the fields are well understood at all the electric conductivity boundaries, so the problem lends itself to the use of standard numerical techniques for determining the fields at all other points in the model.

The finite difference code of Brewitt-Taylor and Weaver (1976) is being used initially to investigate the electric conductivity structure of the continental margin of south-east Australia. The pattern of electromagnetic induction in the region is dominated by the Geomagnetic Coast Effect so the models produced are expected to highlight some aspects of its origin.

COMPACT FINITE ELEMENT METHODS APPLIED TO 3-D TRANSIENT EM MODELLING

A.P. Raiche
CSIRO Division of Mineral Physics and Mineralogy
PO Box 136, North Ryde, NSW 2113, Australia

The computation of the transient electromagnetic (TEM) response of a three-dimensional target in a conducting host requires the solution of the 3-D vector diffusion equation (VDE) either explicitly or in alternative forms. At the outset, one is faced with two choices: the time-stepping approach in which one solves the equation directly; or a frequency-stepping approach in which discrete frequency solutions to the 3-D vector Helmholtz equation (VHE) are combined and transformed into the time domain. The latter is considerably easier to implement and control than the former. It forms the basis of what follows.

Solutions to the VHE are calculated in the range 10 Hz - 10 KHz at a logrithmically-spaced density 5 or 6 frequencies per decade. The frequency range is extended upward until the target response is negligible compared with the host response; i.e. when the depth of burial greatly exceeds the skin depth of the incident radiation. Similarly, the frequency range is extended downward until the incremental total response is negligible; i.e. the wave length of the incident radiation is much greater than the target size. For the targets studied to date, the usual range has been 0.1 Hz to 25 KHz requiring 25 to 30 solutions to the VHE.

The frequency domain response to a step current turn-off is constructed using a cubic spline interpolator combined with analytic solutions for the host at high frequencies. The imaginary component is transformed into the time domain using linear digital filters. This resulting time-domain earth response function is convolved with transmitter and receiver characteristics to yield the predicted response of either existing or hypothetical TEM systems.

The method is dependent upon finding effective solutions to the 3-D VHE. In principle, solutions could be obtained using standard finite element/difference techniques. In a non-Cray environment, the implied computing times are unacceptable. Moreover, simulating the boundary at infinity with homogeneous Dirichlet or Neumann conditions on the boundary of a finite mesh can lead to spurious and often unpredictable effects.

For a class of problems where the host consists of horizontal layers of uniform properties containing a localised heterogenious region, a boundary condition at infinity is no longer required. The compact finite element method consists of placing an artificial boundary just outside the heterogeneous region and solving a set of finite element equations simultaneously with an integral equation on this boundary.

If the induced currents in the heterogeneous region were known, the Green's tensor could be used to calculate the electromagnetic fields everywhere outside this region, and in particular, on the boundary. On the other hand, if the electromagnetic fields were known on the boundary, the finite element method could be used to calculate the internal fields and hence the induced scattering current. Solving these two problems simultaneously allows the fields and currents to be calculated everywhere. For the models investigated so far, the compact finite element method has performed quite well for conductivity contrasts not exceeding 300 to 1.

The high contrast problem is caused by a numerical imbalance between the curl-free and divergence-free current modes. We expect to be able to extend

the contrast range by using higher order basis functions for the finite element part. No results are yet available.

The question of discretisation criteria remains a difficult one. All of the work to date has used a uniform mesh. However, the solutions to the VHE can be viewed as solutions to an inverse problem with perfect data (the EM fields in the absence of the scatterer). The inverse problem was to find the coefficients of the linear or quadratic functions which best represented the scattered field in each finite element. This approach can be extended to finding the best locations for each finite element node. This point is important since it is known that the scattering currents are concentrated near the edges of conductive targets at high frequencies (early delay times) and tend to be more uniformly distributed for low frequencies (late delay times).

Starting with a uniform mesh at low frequencies, least squares inversion procedures can be used to determine node positions subject to the constraint that the node density must increase towards the target edge in a monotonic fashion with increasing frequency. For solutions to the VDE, this inverse approach is designed to allow a time-varying finite element mesh to conform to the diffusion current pattern in a controlled fashion. The relationship between this approach and the moving finite element work going on at Los Alamos is not yet understood since results from neither is yet available.

Smooth Particle Hydrodynamics

Robert A. Gingold
Mount Stromlo and Siding Spring Observatories
ANU

A novel technique for investigating multi-dimensional compressible fluid flows will be described. The method is a grid-free Lagrangian particle code which uses kernel estimation to recover the physical fields at any point in space and has been called Smoothed Particle Hydrodynamics (SPH). In contrast to many other particle codes, the relationship between the equations governing the properties of the particles and the physical equations being solved is known. An animation of a turbulent flow computed with this code will be shown as an example of the type of problem currently being adressed. The basic idea, however, could well be applied to quite different systems of equations and so the talk will concentrate on describing the basis of the method.

HYDROTHERMAL MODELLING STUDIES OF A GEOLOGICAL THERMOSYPHON

Harry P. Schlanger

CSIRO Division of Geomechanics, PO Box 54, Mount Waverley, Victoria 3149.

The thermosyphon principle is used in a diversity of applications such as cooling of transformers, car engines, solar and nuclear reactors. An abundance of the literature forms the subject of several reviews (for example [1]). Relatively few papers describe geological systems or thermosyphons driven by concentrated heat sources.

In this paper, we are interested in solving numerically the temperature distribution and fluid flow in the vicinity of a saturated porous thermosyphon in contact with a low permeability saturated rock mass (Figure 1). The heat source, located in the lower arm drives a natural flow around the loop thereby cooling the source itself and its surroundings. This configuration has practical application in deep burial of nuclear waste [2]. We also investigate the effect of a caprock on flow and temperature distributions due to a point source within a reservoir. The model's caprock permeability is set to that of the reservoir and we investigate the effect of varying reservoir permeability.

Numerical simulations are performed in two dimensions under steady-state conditions with SHAFT79 (Simultaneous Heat and Fluid Transport) which was developed at the Lawrence Berkeley Laboratory [3], and has been adapted on the CSIRONET Cyber205 computer [4]. Based on the integrated finite-difference method, the code solves problems involving transient or steady-state systems for one- or two-phase fluid flow and is designed for one, two, or three dimensions. The user may define zones of different material properties. Output consists of the scalars: temperature, pressure, density, degree of saturation, and the vectors: heat and mass fluxes. Graphical output is produced locally at the CSIRO Division of Geomechanics [4]. Specifically, we are interested in the temperature distribution and mass fluxes (velocity) of the circulating fluid which depend on the power rating of the heat source, and thermosyphon design parameters (eg. loop dimensions, material properties).

The numerical code determines temperatures and flows in both the loop and low permeability rock mass. Analytical parameters that characterize the system are derived if we make a simplifying assumption that heat transfer in the rock mass occurs only by conduction. In this present study, analytical parameters are used in conjunction with numerical results to describe the thermosyphon. A modified Rayleigh number thus obtained is defined for linear flow in the loop as:

$$Ra = \beta g K A_0 L^2 / \nu \lambda \alpha w d$$

where β is the coefficient of thermal expansion, g is acceleration due to gravity, K is permeability, A_0 is the source strength, ν is kinematic viscosity, λ is thermal conductivity, α is effective thermal diffusivity, L is the loop perimeter, w is the loop width, and d is the loop depth. This Rayleigh number simplifies to that defined by Bejan [5] if the geometrical variables are chosen to be interrelated by $d=L^2/w$. However, each system has its own defined set of dimensionless variables.

Figures 2 to Figures 3 are part of preliminary results of a series of SHAFT79 simulations at steady-state showing the effect on flow and temperature of variations in the Rayleigh number by changing loop permeability. A 250 W/m constant flux heat source is embedded at the location shown. The surrounding rock mass has a very low uniform permeability. Thermosyphon permeability was set initially identical to rock mass (Ra=.05), then increased corresponding to Ra=500 and Ra=50,000 respectively. Simulations were performed on a mesh consisting of 12 by

12 elements with 50°C initial and constant temperature boundary conditions. The mass flux results are superimposed on this mesh whereas temperature contours are plotted on a grid with intersections corresponding to element centroids.

Shown in Figure 2a are flow patterns due to the heat source alone, without the thermosyphon. Although convective rolls are evident in the low permeability rock mass, the magnitude of the flows are extremely small and a hot spot with a peak temperature of 112°C occurs at the source (Figure 2b). Temperature contours in the shape of concentric circles around the source are similar to the theoretical results obtained by Bejan [5] for low Rayleigh number convection in an infinite medium. With increase in the loop Rayleigh number, the thermosyphon has greater ability to transport heat away from the system by convection and fluid in the loop circulates at progressively greater velocity, cooling the source to 71°C and 58°C respectively. Figure 3a shows the case Ra=50,000. There are large flows within the loop (note scale change), but the small flows in the rock mass are actually reduced. The corresponding temperature contours in Figure 3b are lowest and curl in the direction of flow around the loop indicating enhanced transport of thermal energy by convection.

Other results show that when a caprock overlies a point heat source, temperature contours take up a mushroom-shape, bunching up just beneath it and restricting convection to below the caprock. In the absence of the caprock, however, convection occurs throughout and temperature contours extend to the surface. The reservoir is cooler. The effect of varying uniform reservoir permeability has shown a result similar to the effect of changing permeability in the thermosyphon. As permeability (Rayleigh number) is increased, there is a transition from very little flow in the reservoir and temperature build-up around the source, to increased flow in the reservoir and lower source temperatures.

So far, our preliminary results have quantified the expected trend of increasing fluid velocity but decreasing temperature as the Rayleigh number is increased. These have been obtained with coarse grids. The next step is to refine grids, and move to three dimensions. We may also investigate how temperature and fluid velocity change with the Rayleigh number if the source is redistributed into smaller amounts around the loop. In conclusion, numerical results have shown that temperatures in the vicinity of a constant flux heat source are reduced as the Rayleigh number is increased. The limiting case of a porous loop in contact with a non-porous rock mass is represented by a Rayleigh number which is different to that defined by Bejan [5] for a point source in an infinite porous medium. We surmise that the general case of a porous loop in contact with a porous medium may be represented analytically by some combination of each Rayleigh number.

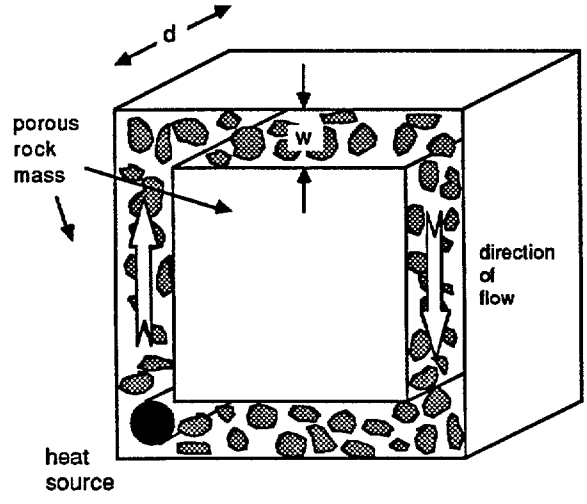

Figure 1
A porous thermosyphon of perimeter L showing location of heat source.

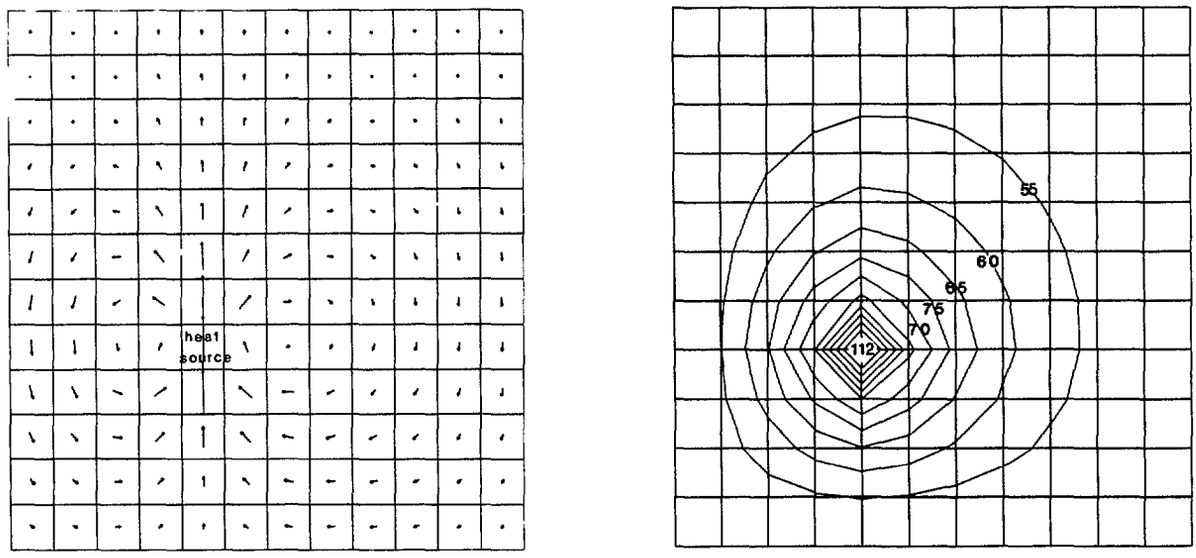

(a) (b)

Figure 2
(a) Flow patterns and (b) temperature contours (°C) for a point source in an infinite porous medium, Ra=.05 .

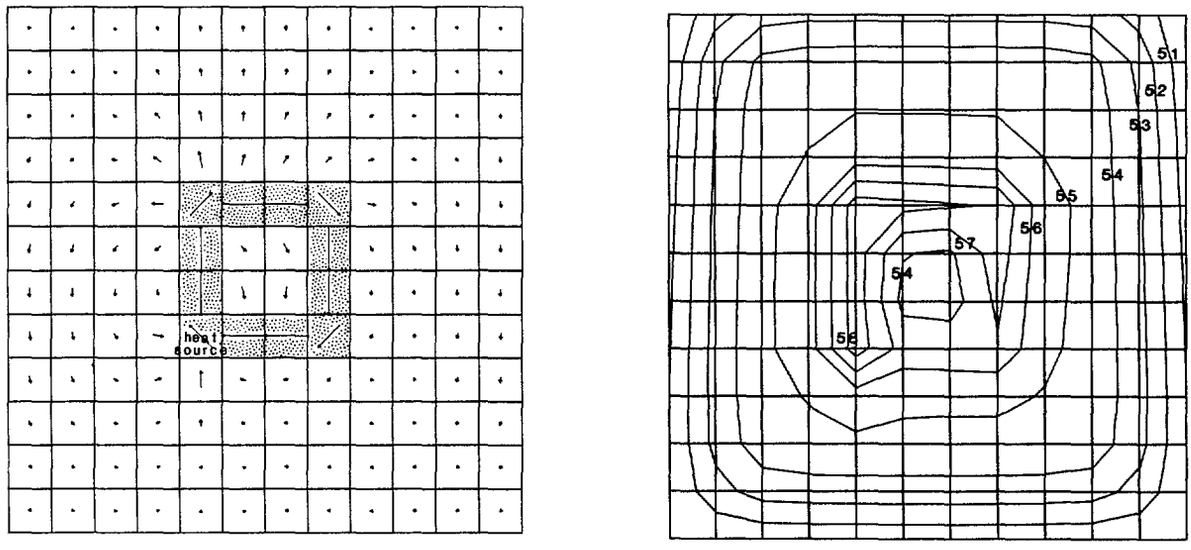

(a) (b)

Figure 3
(a) Flow patterns and (b) temperature contours (°C) for a point source in a porous loop with Ra=50,000 in contact with rock mass. The scale for the vectors outside the loop is 10,000 times greater than for the vectors inside the loop.

References

[1] Zvirin, Y. (1981) Nuclear Eng. Des. 67, 203-225

[2] Brady, B.H.G, Hobbs, B.E., Paterson, L., and Schlanger, H.P. (1986) Proc. 27th US Symp. Rock Mech. Alabama.

[3] Pruess, K. and Schroeder, R.C. (1979) Report LBL-10861 Lawrence Berkeley Lab, Berkeley, Calif.

[4] Schlanger, H.P (1987) CSIRO, Division of Geomech. Tech Report 150

[5] Bejan, A. (1978) J. Fluid Mech. 89, pp 97-107

TWO-DIMENSIONAL MODELLING OF THE PRESENT DAY THERMAL REGIME IN THE SOUTHERN COOOPER BASIN, SOUTH AUSTRALIA

Kerry Gallagher
Research School of Earth Sciences, ANU, Canberra.

The Cooper Basin area of NE South Australia has geothermal gradients (estimated from corrected bottom hole temperatures (BHT) observed in exploration wells) of between 30 and 60° C/km. High gradients are often associated with granitic basement. Knowing the thermal conductivity in the sediments as a function of depth and the BHT the thermal resistance method may be used to estimate the heatflow through the sedimentary pile to the surface. Inherent in this method is the assumption of 1-D steady state (Fig. 1).

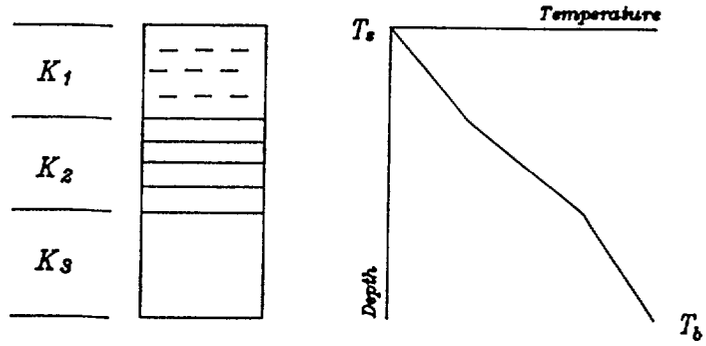

$$T_b = T_s + Q\sum^{n}\Delta Z_i/K_i$$

$$Q = \bar{K}(T_b - T_s)/Z_b$$

$$\text{where } Z_b/\bar{K} = \sum^{n}\Delta Z_i/K_i$$

Fig 1. The thermal resistance method for estimating heat flow. T_S is the (assumed) surface temperature, T_b is the temperature observed at depth Z_b and K_i is the interval thermal conductivity.

However additional downhole temperature data for some wells with granitic basement appear to be inconsistent with this assumption. These temperatures, obtained during drill stem tests, are lower than those expected and the geotherm has a concave up form. Geochemical evidence suggests that the present day thermal regime is a recent (<10 Ma) phenomena. However it can be shown that for a temperature increase at the base of the sediments such that the geotherm is increased from 30 to 60° C/km, steady state is effectively reached in less than 0.25 Ma. The observed temperatures are not attributed to such transient effects.

Although lateral thermal conductivity variations are considered to be small in the sediments, the basement lithologies are more variable. A finite difference scheme in cartesian and cylindrical coordinate systems was used to examine the influence of lateral variations in thermal conductivity and internal heat production on the steady state geotherm. Advective heat transport due to horizontal fluid flow in an aquifer was

simulated in the cartesian coordinate system. Fig 2 shows the general 2-D geometry of the models.

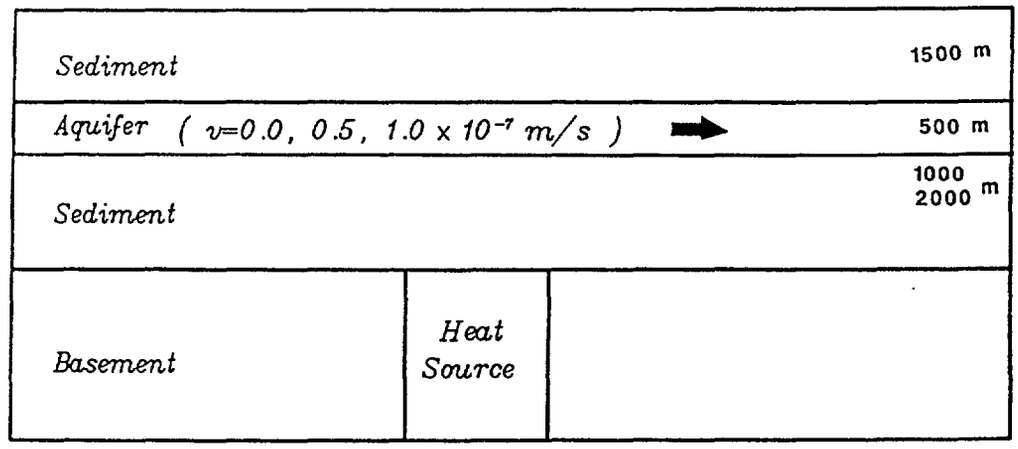

Fig 2. Geometry of the models used. If the advective term is neglected (v=0) the models are symmetrical about the axis of the heat source.

A body with a positive thermal conductivity contrast (ΔK) channels heat upwards as a result of refraction of heat into the body. The geotherm is elevated and heat flow enhanced above the body. A body with a positive internal heat production contrast (ΔH) will obviously increase the vertical heat flow relative to the background but lateral flow now occurs out of the sides of the body. Therefore ΔK and ΔH act in opposite senses to each other with respect to the vertical heat flow anticipated from the 1-D situation. The geometry of the body, height:width or aspect ratio, exerts an important control on the lateral flow of heat and also the depth to the upper surface is a factor as a result of the constant surface temperature condition imposed at the upper boundary of the models. As would be expected, departure from the 1-D situation is greater for a cylindrical body (i.e. pipe like) than a similar width body in cartesian coordinates (sheet like).

For a given positive ΔK, a body with a low aspect ratio tends to result in a steeper average geotherm, although shows less curvature of the temperature profile, than a higher aspect ratio body. For the models considered here, the calculated geotherm, and temperature, is greatest over the middle of the body and reduces towards the margins, although remains high relative to the 1-D case. For a given positive ΔH, the aspect ratio has a similar effect to that mentioned above although the curvature of the geotherm is greater. The lateral flow of heat away from the body means that the value of internal heat production estimated assuming 1-D vertical heat transfer would be too low for a given thickness body and a higher aspect ratio requires a greater ΔH to achieve a given temperature at the upper surface of the body. The effect of steady state advective heat transport in an aquifer is to reduce the temperature at the base of the sediments as the velocity of flow increases, and the geotherm is slightly steepened. However negligible curvature is observed. Heat flow values estimated from BHT and the thermal resistance method should be treated with caution. However they may be regarded as minimum (or maximum) estimates of the heat flow from the basement into the base of the sediments if the geotherm can be demonstrated to be concave up (or down) relative to that expected for the 1-D case. Fig 3 shows geotherms over the centre and at the margin of a body at 4 km with

positive ΔK and ΔH and the geotherm that would be calculated using the thermal resistance method and the BHT, or temperature at the base of the sedimentary pile here.

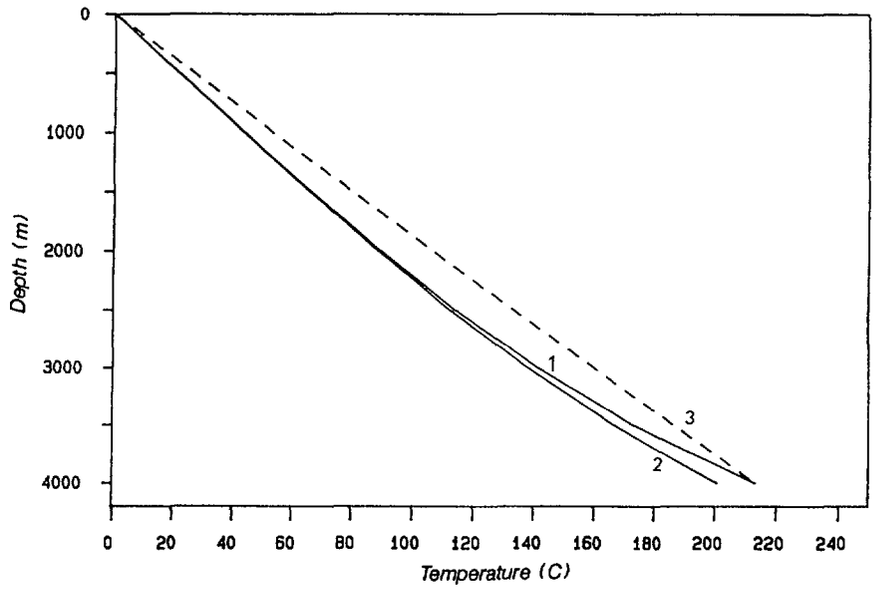

Fig 3. Model geotherms over the axis (1) and the margin (2) of a body with positive ΔH and ΔK. The dotted line (3) illustrates the geotherm that would be derived using the thermal resistance method and the temperature at 4000 m.

MODELLING OF HIGH-T METAMORPHISM AND COEVAL NAPPE TECTONICS IN THE MOUNT ISA INLIER, AUSTRALIA

Ramon J.H. Loosveld

Geology Department, Australian National University, A.C.T. 2601, Australia

Although it is widely believed that as a direct result of crustal thickening geothermal gradients become shallower, a wide variety of fold belts has undergone high-T/low-P metamorphism during their formation. Explanations offered for these anomalously high paleo-geothermal gradients include (1) syn- to slightly pre-metamorphic lithospheric extension (Wickham & Oxburgh, 1985), (2) radioactive selfheating due to thickening of the crust in combination with slow erosion (England & Thompson, 1984) and (3) various magmatic events (Wells, 1980). Subsequent to the prograde high-T metamorphism, Early to Middle Proterozoic fold belts of Australia have undergone isobaric cooling, resulting in an unusual anti-clockwise P-T-t path. As an explanation Etheridge et al. (1987) proposed (4) crust-mantle delamination coupled with the upwelling of hot asthenospheric material to the base of the crust. In this study, the thermal effects of these various situations have been one-dimensionally approximated, using a finite-difference technique. The partial differential heat equation is approximated numerically by an implicit (Crank-Nicolson) finite-difference scheme. The computation here is iterative rather than by direct matrix solution and is tackled using (either interpreted or compiled) MacBasic™ on a Macintosh Plus. Results were then compared to the P-T-t data of the Mount Isa Inlier.

(1) Wickham & Oxburgh (1985) linked steep paleo-geothermal gradients, affecting large areas, with continental rifting: mantle diapirism would result in partial melting of the lower crust, emplacement of granodiorites in the middle crust and a condensed series of isograds. The thermal relaxation of such an event will be, however, too short-lived to be of much influence during metamorphism in the Mount Isa Inlier (>100Ma. later), except around fractionated felsic granites in which heat producing elements (HPE) have been concentrated. The permanent thermal anomaly around these can easily lead to local prograde sillimanite-blastesis. This leaves two problems: firstly, in the inlier high-T metamorphism is not local; secondly, although the initial geothermal gradient could be steep, the P-T-t path from incipient crustal thickening onwards can be expected to be (normal) clockwise.

(2) Among many others, England & Thompson (1984) have stressed the possibility of "radioactive selfheating", i.e. the reaching of high T/P ratios in a collisional zone due to the thickening of the HPE-enriched crust. Additional complexities like frictional heating and relaxation of a crust with a heterogeneous vertical thermal conductivity distribution can locally further condense the isotherms. With certain favourable parameterisations, geotherms can for some time transect the andalusite-sillimanite field. P-T-t paths resulting from such crustal thickening, however, will be clockwise and can only transect the andalusite/sillimanite field in a retrograde way, unless unrealistic parameters are assumed, e.g. a very low conductivity, high radioactive heat production, high basal heat flow, introduction of "magmatic or hydrothermal heat" and the assumption of the presence of eclogite- or other high-density-sinkers.

(3) Wells (1980) studied the thermal effects of crustal thickening by magmatic accretion, i.e. both under- and over-accretion. Rocks above the intruded material will isobarically or slightly decompressively heat up and, during the later stages of thermal relaxation of the magmatically thickened crust, isobarically or decompressively cool. Again the thermal anomalies are short-lived, unless an extra factor for HPE-enrichment is added to Well's models. In the Mount Isa Inlier, however, pre- and syn-tectonic igneous rocks do not seem to be voluminous enough to solely explain the widespread high-T metamorphism.

(4) Relaxation paths after crust-mantle delamination with the upwelling of asthenospheric material to the base of the crust were calculated. Both ongoing convection in the anomalously shallow asthenospheric material, and immediate "freezing" of the asthenospheric material were considered (resp. the "hot mode" and the "cold mode" of Bird & Baumgardner,1981). Considering the "cold mode" delamination and heat transfer in the crust by conduction only, andalusite-sillimanite conditions are not reached on any level. Peak temperatures in the upper crust are reached between 10 and 20 Ma. after delamination. To obtain larger and/or longer-lasting temperature anomalies, another heat source has to be added, either some form of "hot mode" intrusion of the asthenosphere, or radioactive selfheating in a contemporaneously thickened crust, or immediate differentiation of the magmatic products leading to HPE enriched upper crustal slabs.

i Hot mode delamination can lead to andalusite-sillimanite conditions, given a minimum length of time that the intruded asthenosphere can convect.

ii A combination of radiogenic selfheating and cold-mode crust-mantle delamination can also lead to andalusite-sillimanite conditions, but depends strongly on their relative timing. Crustal thickening, instantaneous, and coeval with cold-mode delamination e.g. must be regarded as a very inefficient way of steepening the geothermal gradients, since the time-dependences of the thermal effects of these two tectonic geometries counteract each other: crustal thickening and concomitant radioactive selfheating can only give rise to abnormally steep geothermal gradients if uplift and erosion rates are low. The slower the erosion, the higher the temperatures reached. Peak-temperatures are reached successively later at deeper levels and in many cases more then 30 Ma. will separate the crustal thickening event and the timing of peak-temperatures at a deeper level. By then, however, the thermal relaxation of cold mode delamination will be almost complete.

iii Magmatic differentiation into HPE enriched granites coeval with complementary delamination gives rise to a powerful and permanent heat source and will have two thermal effects: the first one the transient cooling of the magma and concomitant heating of the country rock (contactmetamorphism), the other effect is brought about by the HPE anomaly, which will cause permanent, anomalously high temperatures. The presence of HPE enriched granites in the Mount Isa Inlier encourages a more thorough study into the thermal effects of granitic intrusions and of their source rocks.

All the above exercises have one oversimplification in common: they consider heat transfer by conduction alone. Convection and advection of fluids are at present being incorporated in the models.

REFERENCES

Bird, P. & Baumgardner, J., 1981. Steady propagation of delamination events. **J. Geoph. Res., V. 86, No. B6**, 4891-4903.

England, P.C. & Thompson, A.B., 1984. Pressure-Temperature-Time paths of regional metamorphism I. Heat transfer during the evolution of regions of thickened continental crust. **Journal of Petrology, V.25, part 4**, 894-928.

Etheridge, M.A.E., Rutland, R.W.R. & Wyborn, L.A.I., in press. Orogenesis and tectonic process in the Early to Middle Proterozoic of northern Australia. **Am. Geophys. Union., Geodynamic Series.**

Wells, P.R.A., 1980. Thermal models for the magmatic accretion and subsequent metamorphism of continental crust. **Earth and Planetary Science Letters, 46**, 253-265.

Wickham, S.M. & Oxburgh, E.R.,1985. Continental rifts as a setting for regional metamorphism. **Nature, 318**, 330-333.

A FINITE DIFFERENCE METHOD FOR 1-DIMENSIONAL GEOHISTORY ANALYSIS

by

Michael Swift

Thermal geohistory analysis is a method whereby structural, subsidence, oil maturation and temperature histories can be calculated from a sedimentary section. The thermal calculations have usually depended on a variety of analytical solutions for the heatflow equation. While this approach is adequate for a 'first look' in a region of simple geological and thermal development it is not applicable in the general case because of the assumptions and simplifications required to derive the describing analytical functions.

The heatflow equation is a linear parabolic partial differential equation of second order and in one space dimension, for a compacting sediment it is described by:

$$[\rho_w c_w \phi + \rho_s c_s (1-\phi)]\,\partial_t T = \partial_z (K \partial_z T) - \partial_z [(\rho_w c_w V_w \phi + \rho_s c_s V_s (1-\phi)) \cdot T] + A$$

The first component on the right hand side is the conductive component, the second is the advective component and the third the contribution of heat due to radioactive decay. As the equation is time dependent it requires both an initial condition and subsequent time dependent boundary condition for solution. Analytical solutions to the equation above generally require that basement heatflow as a function of time be known and that it varies slowly with respect to the diffusion timescale of the sedimentary section. Further the advective component is neglected and so eliminating the dynamic development of the sedimentary section, and finally the remaining conductive factor is simplified by finding an average thermal conductivity. In all the initial and boundary conditions may not be at all representative of the real

geological picture. The most feasible method to solve the transient heat flow equation in the general cast is by numberical methods. It is easy to replace the partial differential equation of heat flow by a finite difference equation using the backwards implicit method. The solution is well posed, consistent, convergent and stable and only suffers from truncation errors. A non-uniform mesh can be used to form the grid on the area where the physical parameters change rapidly and as the method requires the solutions of simultaneous linear algebraic equations where the matrix coefficient is tridiagonal it is easy to solve by Gaussian elimination, which has good round off characteristics. In comparing and contrasting the solutions by analytical and numerical methods there is little difference in simple cases. However in the general case the effects of sedimentation, variation in background heatflow, advection and changes in intial conditions such as the conductivity profile can produce marked differences. Notable, sedimentation reduces subsurface heat flow and so delays oil maturation, there is also a time lag between background heatflow changes and the heatflow within the sedimentary section. The size of the lag depending on whether the variation takes place at basement depths or at the base of the crust or the base of the lithosphere. Heat transfer by advection is marked in highly porous rocks and the conductivity profile has a direct influence on the sediment temperature.

To summarize the benefits of the numerical approach, it has greater versatility in dealing with complicated space dependent variables such as thermal conductivity, porosity, density, heat capacity as well as time dependent boundary conditions such as background heatflow, and surface temperature. The dynamic processes active in the development of a sedimentary section, such as compaction, water advection, sedimentation rates are all considered when calculating the thermal history of the sedimentary column.

NUMERICAL METHODS IN DYNAMIC HYDROTHERMAL MODELLING OF THE RENISON TIN MINE, TASMANIA

Peter William Holyland

Department of Geology and Mineralogy, Uni. of Queensland, Brisbane

Cassiterite mineralisation at the Renison tin mine, Tasmania, is spatially and temporally related to the Upper Devonian Pine Hill Granite, and occurs as replacements of chemically favorable flat lying dolomite beds and infills of major faults which connect the dolomites to the underlying granite. Exsolved magmatic fluids from the granite, which contrast with the wallrocks in pressure, temperature and chemical potential, have reacted chemically and interacted mechanically with the wallrocks to form the orebodies.

A number of analytical and numerical models have been applied to the hydrothermal system to simulate the transport of mass, momentum, and energy from source to sink areas, and also the fluid/rock transfer. The aim has been to constrain the controls on dolomite replacement.

The first of these models uses a simple 2D finite difference method to obtain solutions for time dependant potential flow. Pressure buildup in the Mine Granite, resulting from magmatic volatile exsolution, was dissipated along a vertical narrow high permeability zone (Federal-Bassett Fault) into the sub-horizontal layered Mine Sequence. Volatile exsolution rate is assumed to decay exponentially due to the increasing downdraw in the magma reservoir and the depth dependance of solubility (Burnham,1985).

Total flux-pressure paths for a number of the discharging faults, estimated from mass transfer and inelastic deformation textures in the Mine Sequence, confirm the exponential model, and were used to calibrate the pressure buildup accompanying mineralisation.

The second model uses a finite difference method to obtain solutions to the governing equations for multicomponent reactive flow through porous media. The algorithm used is designed to simultaneously satisfy the minimisation of Gibbs free energy, the equilibrium condition, and the mass balance constraints for a closed chemical system. Input data includes a list of the species present in the dolomites before and after reaction, the standard free energies of formation of these species, the molar amount of each element in the system, and initial estimates for the species which satisfy the element abundance constraints.

The physical model used to describe the flow of granite derived fluid into the dolomites assumes uniform boundary conditions (Riemann problem). The model is one dimensional and divides the dolomite into a number of equally spaced grid blocks, with the first block representing the injected conditions. The rate of flow is assumed to be less than the reaction rate and hence fluid/rock local equilibrium is attained in each block.

Composition and temperature of the injected fluid was estimated from fluid inclusion bulk leachates sampled in the feeder faults by Patterson et al.(1981). Similarly, initial conditions in the dolomites were estimated from modal analyses and XRD determinations of the carbonate speciation.

The solution obtained is characterised by composition changes or waves moving through the dolomite, separating regions of constant composition. Simulated mineral assemblages in these zones correspond closely to the dolomite, calcite, hydrothermal carbonate (siderite) and massive sulphide zones mapped in the field, while a previously undefined zone, predicted by the simulations, has subsequently been verified. Specific wave velocities, or relative zone dimensions, indicate that permeability distribution in the dolomites was anisotropic and heterogeneous, primarily controlled by pre-existing D2 minor fold axes and axial faulting.

REFERENCES

Burnham C.W., 1985. Energy release in subvolcanic environments: implications for breccia formation. Economic Geology v80 p1515-1522.

Patterson D.J., Ohmoto H., and Solomon M., 1981. Geologic setting and genesis of cassiterite-sulphide mineralisation at Renison-Bell, Western Tasmania. Economic Geology v76 p393-438.

A Simulation of Fabric Development in Dynamically Recrystallising Rocks

Mark Jessell

Dept. of Earth Sciences, Monash University, Clayton, VIC, 3168.

Recent advances in the understanding of dynamic recrystallisation processes have enabled a new attempt to be made at creating a general model of fabric development in rocks. A new two-dimensional Monte Carlo simulation of the development of crystallographic and grain shape fabrics is presented here, and analogies will be drawn between the fabrics predicted by this simulation and those found in naturally and experimentally deformed rocks.

This model is based on the interaction of three deformation processes, namely progressive straining, the lattice rotations induced by crystal glide, and two types of dynamic recrystallisation. The foundation of the simulation is a triangular array of points, in which each point represents a discrete area of material, and has an associated c-axis orientation. The various deformation processes act either on the relative positions of these points or on their particular lattice orientations, and the deformation of the material is simulated by the successive repetition of these incremental processes.

Although this model is characterised by being more complicated than sophisticated, on comparison with previously measured fabrics, it can account for aspects of fabric evolution that could not be explained using established models. In particular it predicts the development of the variously positioned c-axis point maxima found in naturally deformed rocks, and gives a possible explanation for the evolution of fabrics from one strong pattern to another with progressive deformation.

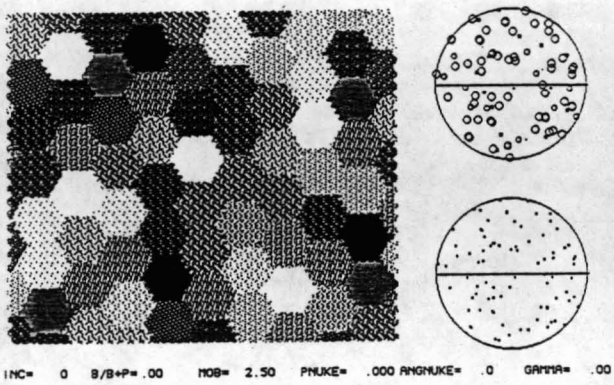

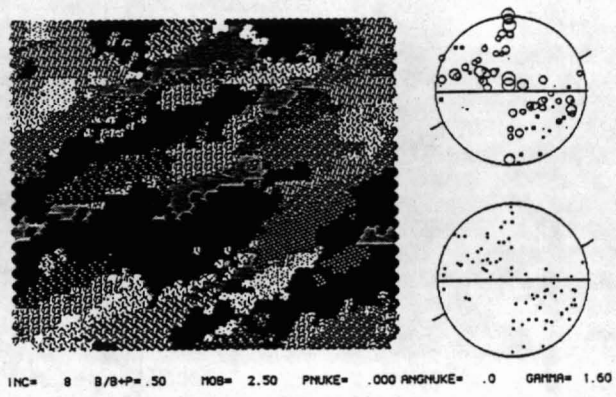

GROUNDWATER MODELLING OF THE RIVERINE PLAIN, SOUTH-EASTERN AUSTRALIA

J. G. Nolan
Department of Industry, Technology and Resources
Geological Survey, Groundwater Branch, Melbourne

Since European settlement the Riverine Plain of the South-Eastern Murray Basin has undergone drastic landuse changes to become one of Australia's most productive agricultural regions.

The long-term viability of the region is now threatened by land salinisation and waterlogging; a direct result of increased rates of recharge in response to land clearing of natural vegetation and irrigation.

In an endeavour to minimise agricultural losses, several management control strategies have been proposed. To evaluate the physical and economic viability of these strategies a suite of integrated numerical models are being established. These include regional 3-D, sub-regional 3-D and sectional 2-D groundwater flow models in addition to district 2-D solute transport models.

The USGS modular three dimensional finite difference model (MODFLOW) has been employed for most groundwater flow models. This code has been divided into modules, which permits the user to examine specific hydrologic features of the model independently. This also facilitates development of additional capabilities because new modules or packages can be added to the program without modifying the existing modules or packages. The input and output systems of the computer program are also designed to permit maximum flexibility.

Groundwater flow within the aquifer is simulated using a block-centered finite-difference approach. Layers can be simulated as confined, unconfined, or a combination of confined and unconfined. Flow from external stresses, such as flow to wells, areal recharge, evapotranspiration, flow to drains, and flow through riverbeds, can also be simulated. The finite-difference equations can be solved using either the Strongly Implicit Procedure or Slice-Successive Over-relaxation.

Due to the significant spatial and temporal variability of the system, as a consequence of seasonal and long term fluctuations in climatic conditions, land use practices and hydrogeological heterogeniety, it has been necessary to conduct an exhaustive investigation to accumulate and collate relevant information into a readily accessible data base. Lithological, stratigraphic, meteorologic, pedologic, topologic, hydrographic and water usage data have been collected for the 15 year period commencing in 1970. Much effort has been spent in synthesising missing records and verification. The data is now in a readily accessible format, and is currently proving invaluable for a wide range of studies in addition to groundwater modelling.

Initial estimations of parameters have been made where direct measurements are not available, and then refined during the calibration phase. These include recharge, unconfined storage and vertical hydraulic conductivities. Recharge has been estimated by a conceptual model based upon the dominant recharge components such as precipitation, irrigation applications, channel intensity and evaporation as well as soil hydrologic parameters.

Two-dimensional sectional modelling along the Goulburn Deep Lead groundwater flow path has been callibrated. This model highlights the significance of the 1973 to 1975 wet period where pressure rises of up to 3 m in the deep lead occurred. Observed watertable rises of between 1 and 3 m are also reflected by the model. Leakage between the watertable aquifer and the deep lead aquifer ranges from 2 mm/year upward in the Wakool, to 7 mm/year downward within the Shepparton Region. Sensitivity studies are now underway to define confidence limits.

This model in addition to other sectional models and a 3-D regional model will now be employed to predict the effect of large scale shallow aquifer dewatering within the Shepparton Irrigation Area, and deep aquifer pumping for water supply throughout the Region where good quality water is available.

MODELLING KINETICS OF PETROLEUM GENERATION IN SEDIMENTARY BASINS - A REVIEW

P.J. EADINGTON
CSIRO Division of Mineral Physics and Mineralogy, North Ryde

The timing of petroleum generation in relation to structure development, fluid migration and diagenesis of reservoir rocks is an important factor in petroleum accumulation in sedimentary basins. Estimating the thermal history of sedimentary basins (Falvey and Deighton, 1982; Waples, 1980) in conjunction with measurement of vitrinite reflectance is often used to model the way organic matter (O.M.) matures through time. O.M. varies in its composition, structure, and in its yield and rate of generation of petroleum. O.M. is routinely measured by microscopy or chemical techniques to interpret in a qualitative way the timing of oil generation. A kinetic model for the generation of petroleum enables quantitative allowance for O.M. type and a rapid experimental method for determination of the kinetic constants for the rocks being investigated.

Generation of hydrocarbons proceeds by cleavage of chemical bonds and molecular rearrangements with changes in concentration (X) of components through time (t) which are typically described by a first order rate law: $dX/dt=-AXe^{-E/RT}$ where the temperature (T) dependence is described by the frequency factor (A) and activation energy (E) that are constants for a particular chemical reaction. R is the universal gas constant.

Direct application of this model is unsatisfactory because there are too few parameters (A,E,X) to describe the sample. A modified approach (Tissot and Espitalie, 1975; Solomon and Hamblen, 1984) considers the oil yield as the sum of products from many parallel reactions each described by first order kinetics. If the kinetic constants (Ai, Ei, Xi) for these reactions can be determined then additional parameters are available to enable description of oil generation under different conditions ranging from laboratory experiments to natural diagenesis.

Changes in the rate at which organic matter is heated cause different reactions to become dominant and the shape of the oil yield curve through time to change. This can be demonstrated with an industrial pyrolysis technique (Rockeval). By fitting the numerical model to several oil yield curves simultaneously the kinetic constants for a range of reactions within one sample can be evaluated (Ungerer and Pelet, 1987). Provided the same reaction mechanisms apply in diagenesis these data can be used as input with the thermal model of a sedimentary basin to estimate aspects of the timing of oil formation in nature.

Monte Carlo simulation and tomographic estimation of seismic velocity.

S.A.Edwards, Department of Earth Sciences, Monash University

Optimization methods are widely used both for the numerical simulation of Earth processes and for the inversion of field data to recover the material parameters governing the evolution of processes. In forward modelling, optimization is carried out via penalty functions which are typically sums of interaction energies, while in inversion, penalty functions are typically Bayesian log likelihoods. In forward modelling, the dynamics of a process may be deterministic or probabilistic. In inversion and imaging, noise and and sampling limitations in field data mean that the material parameters being recovered are only ever known probabilistically. Each new independent item of data measured in the field provides the geophysical interpreter with constraining information about the system being imaged. Each item of information may be modelled as a probability distribution on the set of images permitted by the interpreter's prior parametrization of the system (via pixels, finite elements, parametric models etc.).

The task of an interpreter is to combine partial information into an integrated state of knowledge representable by a final probability distribution which is as sharp as possible in the light of the available field data. A numerical image reconstruction system can assist in this process. In practice the full details of the distribution are not estimated, although estimates of some second moments (covariances) of the distribution are frequently useful, as for example in geostatistical estimation of mineral reserves.

An interactive software system for tomographic estimation of seismic velocity being developed by the CSIRO Division of Radiophysics and Macquarie and Monash Universities takes raw field data (crosshole and offset VSP) and generates a sequence of images representing the velocity distribution in a two-dimensional section through the Earth. The system is being designed to assist the interpreter to find sequences of images of successively greater likelihood in the light of the constraints provided by all available information. Field seismic traces provide quantitative constraints in the form of tomographic travel time estimates along estimated seismic raypaths. Descriptive information is input either graphically by the interpreter or by scanning devices such as CCD cameras.

The design principles of the software system being developed will be discussed in this talk and compared to recent approaches to geophysical inversion by generalized gradient methods (e.g. Gauthier, Virieux and Tarantola 1986, Scales 1987, Kennett and Williamson 1987) and simulated annealing (Rothman 1985).

References.

Gauthier O., Virieux J. and Tarantola A., 1986. "Two-dimensional nonlinear inversion of seismic waveforms: numerical results." Geophysics 51 1387-1403

Scales J.A., 1987. "Tomographic inversion via the conjugate gradient method."

Geophysics 52 179-185

Kennett B.L.N. and Williamson P.R., 1987. "Subspace methods for large-scale nonlinear inversion." Preprint RSES, ANU.

Rothman D.H., 1985. "Non-linear inversion, statistical mechanics, and residual statics estimation." Geophysics 50 2784-2896